Relaxation of Power Ramp Rate Restrictions for ZIRLO Clad Fuel Rods

Technical Report

Relaxation of Power Ramp Rate Restrictions for ZIRLO Clad Fuel Rods

1000847

Final Report, June 2001

EPRI Project Manager
B. Cheng

EPRI • 3412 Hillview Avenue, Palo Alto, California 94304 • PO Box 10412, Palo Alto, California 94303 • USA
800.313.3774 • 650.855.2121 • askepri@epri.com • www.epri.com

DISCLAIMER OF WARRANTIES AND LIMITATION OF LIABILITIES

THIS DOCUMENT WAS PREPARED BY THE ORGANIZATION(S) NAMED BELOW AS AN ACCOUNT OF WORK SPONSORED OR COSPONSORED BY THE ELECTRIC POWER RESEARCH INSTITUTE, INC. (EPRI). NEITHER EPRI, ANY MEMBER OF EPRI, ANY COSPONSOR, THE ORGANIZATION(S) BELOW, NOR ANY PERSON ACTING ON BEHALF OF ANY OF THEM:

(A) MAKES ANY WARRANTY OR REPRESENTATION WHATSOEVER, EXPRESS OR IMPLIED, (I) WITH RESPECT TO THE USE OF ANY INFORMATION, APPARATUS, METHOD, PROCESS, OR SIMILAR ITEM DISCLOSED IN THIS DOCUMENT, INCLUDING MERCHANTABILITY AND FITNESS FOR A PARTICULAR PURPOSE, OR (II) THAT SUCH USE DOES NOT INFRINGE ON OR INTERFERE WITH PRIVATELY OWNED RIGHTS, INCLUDING ANY PARTY'S INTELLECTUAL PROPERTY, OR (III) THAT THIS DOCUMENT IS SUITABLE TO ANY PARTICULAR USER'S CIRCUMSTANCE; OR

(B) ASSUMES RESPONSIBILITY FOR ANY DAMAGES OR OTHER LIABILITY WHATSOEVER (INCLUDING ANY CONSEQUENTIAL DAMAGES, EVEN IF EPRI OR ANY EPRI REPRESENTATIVE HAS BEEN ADVISED OF THE POSSIBILITY OF SUCH DAMAGES) RESULTING FROM YOUR SELECTION OR USE OF THIS DOCUMENT OR ANY INFORMATION, APPARATUS, METHOD, PROCESS, OR SIMILAR ITEM DISCLOSED IN THIS DOCUMENT.

ORGANIZATION(S) THAT PREPARED THIS DOCUMENT

Anatech Corp.

ORDERING INFORMATION

Requests for copies of this report should be directed to the EPRI Distribution Center, 1355 Willow Way, Suite 2478, Concord, CA 94520, Pleasant Hill, CA 94523, (800) 313-3774.

CITATIONS

This report was prepared by

Anatech Corp.
5435 Oberlin Drive
San Diego, CA 92121

Principal Investigator
D. Sunderland

This report describes research sponsored by EPRI.

The report is a corporate document that should be cited in the literature in the following manner:

Relaxation of Power Ramp Rate Restrictions for ZIRLO Clad Fuel Rods, EPRI, Palo Alto, CA: 2001. 1000847.

REPORT SUMMARY

The pellet-cladding interaction (PCI) response of the Westinghouse 17x17-RFA fuel rod design during pressurized water reactor (PWR) startup power ramps was analyzed using the FALCON fuel performance code. Analyses were conducted for both once-burned and twice-burned fuel rods under a variety of power conditions. While study results are consistent with those of previous work, they also extend PCI analyses to include ZIRLO cladding in addition to Zircaloy-4 and expand the evaluation to a wider spectrum of power thresholds and ramp rates.

Background

PWR operators use power ramp rate restrictions during startup following a refueling outage to minimize PCI failures. These restrictions consist of a threshold power level above which a limit on the power ascension rate is imposed. The threshold power levels vary from plant to plant depending on design and can range between 20% and 50% of core full power (EPRI TR-112140-V. 1). A majority of plants use threshold power levels near 20% core power. The power ascension rate below the threshold power is plant-dependent and can vary between 10% to 30%/hr. Above the threshold power level, the most common ramp rate is 3%/hr for core power. Such operating restrictions result in a loss of capacity factor because of the delay in reaching 100% power conditions. Recently, EPRI conducted a program to evaluate and assess the current state of PWR startup conditions following a refueling outage. As part of this program, EPRI performed thermo-mechanical fuel performance analyses to evaluate fuel rod PCI response during a PWR startup as a means to develop a technical basis for relaxing these restrictions.

Objective

To conduct a thermo-mechanical fuel behavior analyses for assessing the impact on PCI failure potential of using relaxed ramp rate restrictions for the Westinghouse 17x17 RFA fuel design operating in McGuire and Catawba nuclear stations.

Approach

To establish the requirements for the PCI power ramp analyses, the research team established base irradiation conditions of once-burned and twice-burned fuel rods. Team members accomplished this by modeling the performance of full-length fuel rods under steady-state (normal base load) operation with Zircaloy-4 and ZIRLO cladding using the fuel rod modeling code, ESCORE. The team then used these base irradiation conditions with FALCON, a fuel performance code, to analyze the PCI behavior of the fuel. Team members developed several scenarios based on power operation and coastdown scenarios compatible with the Catawba and McGuire units. In their scenarios, they evaluated PCI behavior of the W17x17 RFA fuel rod with Zircaloy-4 (reference material) and ZIRLO claddings for a variety of power ramp rates and thresholds. Analyses with the Zircaloy-4 cladding enabled a comparison with previous analyses and allowed researchers to determine a reference point for comparison with the ZIRLO cladding model.

Results

Study results indicate that a threshold of 20% full power (FP) with a post-threshold power ramp rate of 3%/hr is conservative with substantial margin to PCI failure. Analyses further show that an increase in peak cladding stresses occur beyond a threshold of approximately 70% FP at the same post-threshold ramp rate of 3%/hr. Likewise, cladding stresses only increase slightly when the ramp rate increases to approximately 5%/hr for threshold values below 70% FP. These results indicate that some relaxation of ramp rate restrictions are possible without significantly increasing the potential for fuel rod failure by PCI. This relaxation may include increasing the threshold power to 50-60% core power and subsequent power ramp rate of 5%/hr. Such relaxation of ramp rate restrictions apply to ZIRLO cladding as well as to Zircaloy-4 cladding under the same power ramp conditions. Since the analytical evaluation assumed that ZIRLO has the same PCI characteristics as Zircaloy-4, uncertainties may exist that require additional PCI resistance data for ZIRLO.

EPRI Perspective

The objective of identifying less restrictive startup conditions is to gain additional plant capacity without compromising fuel reliability. Use of less restrictive power ramp rate conditions can decrease the time required to achieve full power operation and, therefore, has a potential cost benefit to operating utilities. This particular PCI assessment can be used as part of the technical bases for modifying the current startup ramp rate restrictions at McGuire and Catawba nuclear stations. Similar technical analyses may be applied to other PWRs for modifying their startup ramp rate limits.

Keywords

PWR
Plant startup
Ramp rate

CONTENTS

LIST OF FIGURES

LIST OF TABLES

1
INTRODUCTION

1.1 Background

Operators of pressurized water reactors (PWRs) employ some type of power ramp rate restrictions during startup following a refueling outage. Fuel vendors imposed such operating restrictions in the late 70's to minimize the occurrence of Pellet-Cladding-Interaction (PCI) failures. These restrictions consist of a threshold power level above which a limit on the power ascension rate is imposed. The threshold power levels vary somewhat from plant to plant depending on design and can range between 20% and 50% of core full power (EPRI TR-112140-V1, Ref. 1). A majority of the plants use threshold power levels near 20% core power. The power ascension rate below the threshold power is plant dependent and can vary between 10% to 30%/hr. Above the threshold power level, the most common ramp rate is 3%/hr for core power. Operating restrictions of this nature result in a loss of capacity factor because of the delay in reaching 100% power conditions.

Recently, EPRI conducted a program to evaluate and assess the current state of PWR startup conditions following a refueling outage. As part of this program, EPRI performed thermo-mechanical fuel performance analyses to evaluate the fuel rod PCI response during a PWR startup as a means to develop a technical basis for relaxing these operating restrictions (EPRI TR-112140-V2, Ref. 2). These analyses demonstrated that some relaxation of ramp rate restrictions are possible without increasing significantly the potential for fuel rod failure by PCI. However, the analytical evaluation was performed for Zircaloy-4 cladding and specific plant operating conditions, and as a consequence, may not apply to other fuel rod designs or plant operating strategies.

This report summarizes the thermo-mechanical fuel behavior analyses conducted to assess the impact on the PCI failure potential of using relaxed ramp rate restrictions for the Westinghouse 17x17 RFA fuel design operated in McGuire and Catawba. The main objective of this evaluation is to provide the technical bases for recommending modified power ramp conditions, i.e. threshold power levels and ramp rates, which are less restrictive. The use of less restrictive power ramp rate conditions can decrease the time required to achieve full power operation and therefore has a potential cost benefit to operating utilities.

An important element of this analysis was to evaluate the influence of ZIRLO (Zr-1Nb-1Sn-0.1Fe) cladding on the PCI failure potential for the Westinghouse 17x17 RFA fuel design. This particular fuel design, targeted for operation in McGuire and Catawba, will contain ZIRLO cladding material. There are several key differences between Zircaloy-4 and ZIRLO cladding material, including the yield stress and thermal creep properties that may affect the mechanical and PCI response of the cladding during power ramp conditions. At present, power ramp test data that can be used to quantify the performance of ZIRLO cladding under PCI conditions is unavailable in the open literature. As a result, it is necessary to include an analytical assessment of the ZIRLO material differences on the fuel rod PCI response.

The PCI assessment reported herein can be used as the technical bases for modifying the current startup ramp rate restrictions used in McGuire and Catawba. The objective of identifying less restrictive startup conditions is to gain additional plant capacity factor without compromising fuel reliability. This evaluation must be coupled with a cost benefit analysis and an assessment of the plant operating practices to determine the feasibility of implementing the recommended improved threshold and ramp rate.

1.2 Operating and Economic Benefits

The motivation for increasing threshold and ramp rate is to reduce the time required to achieve full power during the startup phase of the plant, and thus increase the capacity factor, or energy generated during the cycle. Figure 1-1 provides a comparison of two combinations of increased thresholds (50% FP and 60% FP) and ramp rate (5%/hr) with the baseline conditions of a threshold of 20% and ramp rate of 3%/hr. These data exclude hold times at constant power, since it is assumed they would be the same for all power trajectories. By increasing the threshold to 50% with a post-threshold ramp rate of 5%/hr, the energy generation increases by 7.52 effective full power hours (EFPH) as compared to the baseline case. For a threshold of 60% and a subsequent ramp rate of 5%/hr, the energy generation increases by 8.27 EFPH, or 0.344 EFPD.

1.3 Methodology

In order to establish the conditions for the PCI power ramp analyses, a set of steady-state analyses of a full-length fuel rod with Zircaloy-4 and ZIRLO cladding were performed using the fuel rod modeling codes, ESCORE and FALCON. ANATECH developed several power histories based upon the full power operation and several different coastdown scenarios that are considered possible for the Catawba and McGuire units. The results of the steady-state analyses were then used to initialize the analyses of the PCI behavior of the fuel.

The PCI behavior of the W17x17 RFA fuel rod with Zircaloy-4 (reference material) and ZIRLO claddings was evaluated for a variety of power ramp rates and thresholds. The analyses with the Zircaloy-4 cladding enabled a comparison with previous analyses, in order to assure that the methodology was consistent with previous analyses. In addition, the behavior of the Zircaloy-4 cladding determined a reference point with which to compare the ZIRLO cladding model.

The analyses also establish a baseline for the fuel performance with current practices, threshold of 20% of full-rated power and a power ascension rate of 3% per hour above the threshold, with those proposed for the future. The analyses are conservative in the sense that the lower creep rate for ZIRLO was applied to the total creep as opposed to only the thermal creep. The results show that ZIRLO cladding behaves as well as Zircaloy-4 cladding under the same power ramp conditions.

The results of the analyses indicate that current restrictions can be relaxed without necessarily decreasing fuel reliability. The threshold may be relaxed up to 60% of core rate power, or approximately 6 to 6.5 kW/ft on a local LHGR basis, and the post-threshold ramp rate may be increased to 5% (or approximately 0.5 kW/ft/hr on a local LHGR basis). ZIRLO shows a slight increase in stress as compared to Zircaloy-4, but this increase is not so significant as to cause a decrease in fuel reliability.

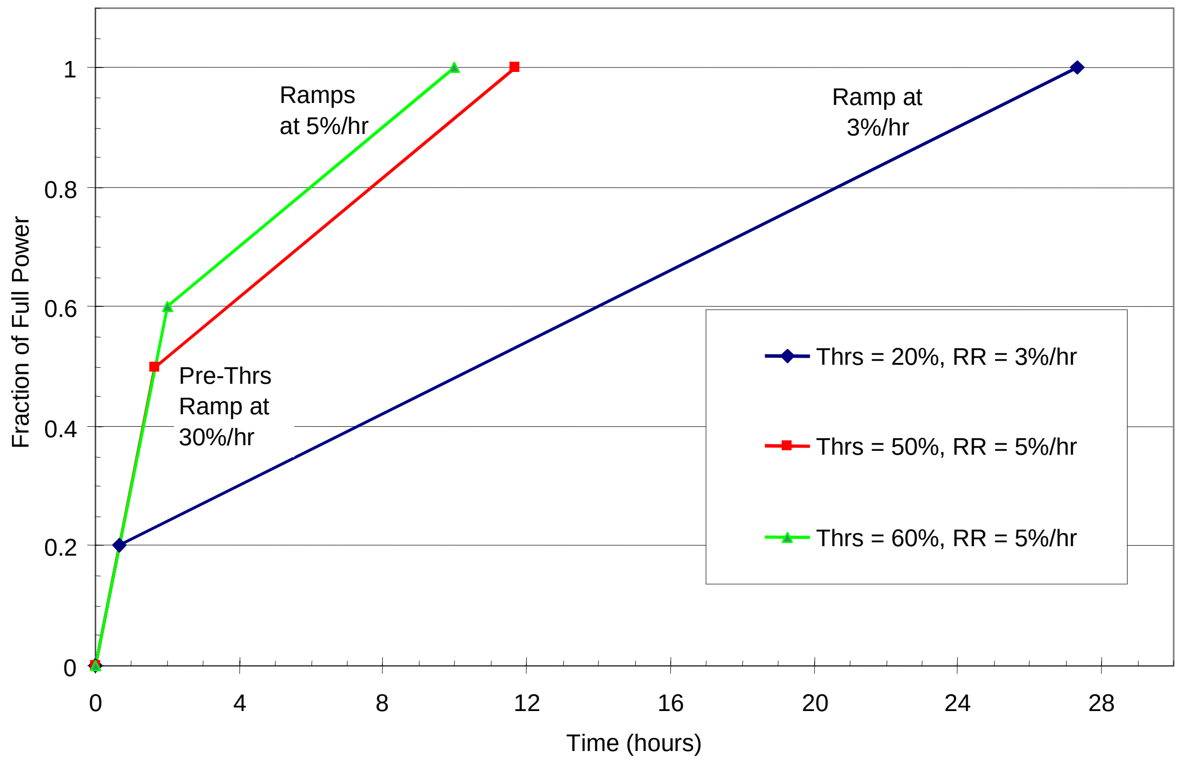

Figure 1-1
Comparison of Faster Startups using Higher Threshold of 50% FP and 60% FP and a Ramp Rate of 5%/hr with the Baseline Startup Conditions of a 20% Threshold and 3%/hr Ramp Rate.

2
METHODOLOGY: ANALYTICAL CODES AND MODELING APPROACH

The analytical tools and modeling approach, which are used to evaluate the PCI behavior of irradiated PWR fuel rods during a reactor startup following a refueling outage, are the same as those reported in Ref. 2, except that the FALCON code (an improved version of FREY) has replaced the FREY fuel modeling code.

The modeling approach consisted of two steps. First, the condition of the peak power fuel rod was established at the end of one and two cycles of operation, once-burned or twice-burned fuel, respectively. This step was accomplished using the ESCORE steady-state fuel performance code. In order to support the ESCORE steady-state calculations, a set of parallel calculations was performed using a preliminary version of the FALCON fuel performance code. Second, the PCI behavior during reactor start-up was established for either the second or third cycle of operation. The second step was performed using the PCI capabilities (a local effects model in the R-θ geometry) of the FALCON fuel behavior program combined with the most conservative initial conditions provided by ESCORE and FALCON.

The following provides a brief discussion of the ESCORE and FALCON programs, the method used to initialize FALCON with the results from ESCORE, and the analysis approach used in the project.

2.1 ESCORE Description

ESCORE is a best-estimate FORTRAN computer code that calculates the steady-state response of an LWR fuel rod. The code calculates both the thermal and mechanical response of a fuel rod as a function of time-dependent rod power. ESCORE's applications include, but are not limited to fuel design, and technical specification and setpoint licensing.

ESCORE was designed to perform best-estimate predictions of fuel rod behavior across a broad range of steady-state conditions, and as such, provides the user with a versatile tool that can be used to evaluate numerous operational alternatives. Computationally, ESCORE calculates the steady-state thermal and mechanical response of a fuel rod by approximating it as a series of discrete, axial segments, accounting for local conditions such as the effects of burnup and temperature on fuel fission-product composition, axial densification, and fuel-cladding gap size. The thermal and mechanical solutions are coupled to provide the overall fuel rod solution. For the thermal computations, independent radial thermal-equilibrium calculations are performed for each axial segment. These are then coupled over the length of the entire fuel rod with the assumption of complete mixing of the free gases within the rod. For the mechanical solution, ESCORE calculates the hot and cold internal rod pressures, the rod internal open void volume, the fuel and cladding outer and inner diameter changes for each axial segment (and the fuel-cladding gap), and the axial fuel and cladding length changes.

Required inputs to initialize ESCORE include the fuel rod geometric parameters, the actual or projected irradiation history, and the core thermal-hydraulic conditions. The fuel rod power history is input as local power that is a function of either axially averaged burnup or time in user-supplied time steps. Burnup is calculated where time is the independent, user-input variable. Alternatively, time is calculated if burnup is the independent, user-input variable. Core average linear heat rate, a radial peaking factor, and an axial power shape can be input at each time step to calculate local rod power. Three options are available to calculate cladding outer-surface temperatures. The recommended first option is to input subchannel geometry, coolant inlet temperature, coolant pressure, and coolant mass flow rate and allow ESCORE to calculate the cladding outer-surface temperature assuming a closed subchannel with either single-phase convection, subcooled boiling, or saturated flow boiling. The heat transfer coefficient is calculated with either the Dittus-Boelter or Jens-Lottes correlations. The second option is identical to the first with the exception that the user supplies the "convective" and "boiling" heat transfer coefficients rather than use those calculated by ESCORE. The third alternative requires the user to directly input the cladding outer-surface temperature at each axial node and at each timestep. For further information on ESCORE's fuel rod modeling technique, input requirements, output information, code structure, and calculational procedure, a detailed description is available in the ESCORE Theory and User's Manuals [Refs. 3, 4].

2.2 FALCON Description

The FALCON code (an enhanced version of FREY) provides a fuel rod evaluation system for the transient and steady-state analysis of light water reactor fuel. FALCON models the thermo-mechanical behavior of a single fuel rod, in detail, utilizing a closed-channel thermal-hydraulic simulation of the rod-coolant heat transfer. In addition, it provides the capability of user-defined heat transfer coefficient and bulk temperature as functions of position and time, thus extending the program's utility to a wide range of transients for which passive coupling of thermal-hydraulic and thermo-mechanical responses is valid. As a general-purpose fuel rod evaluation system, FALCON contains models for best-estimate predictions as well as licensing evaluation.

An important area of fuel performance evaluation in which FALCON provides unique capabilities is pellet-cladding interaction (PCI). It provides a comprehensive tool for diagnostic analysis of PCI-related problems, such as the determination of failure threshold, the evaluation of the effects of ramp rates, power cycling and abnormal power maneuvers on fuel failures, and the assessment of cladding defects on fuel rod integrity.

The theoretical foundation of FALCON is derived from basic principles. The program utilizes the MATPRO material models and the computational structure is based on the finite element method with a backward time difference stepping procedure. Deterministic failure models for cladding integrity evaluations are provided for application to design basis transients, as well as normal, steady-state operation. Under steady-state conditions, a cladding failure criterion based on ISCC is used; for transients, cladding failure is predicted using a cladding rupture criterion.

The failure analysis method utilizes a cumulative damage concept. For safety evaluation under accident conditions, cladding rupture and oxidation criteria are applied to large deformation ballooning-type failures at high temperatures.

FALCON contains models for steady-state analyses to define transient initial conditions or fuel diagnostic evaluations. These models include fission gas release, burnup, fuel cracking and relocation, local gap thickness and conductance, cladding and fuel visco-plasticity, fuel hot-pressing, swelling and densification, and pellet-cladding interaction (PCI). Because of FALCON's finite element structure, these calculations can be carried out for full-length rods, short segments, or slices. FALCON provides geometric models in r-z or r-θ grids as appropriate. FALCON's PCI analysis capabilities are unique in that it permits the detailed simulation in the r-θ plane of discrete pellet cracks and pellet-cladding interfacial forces. The following is a list of parameters, computed by FALCON, which are generally needed for licensing and fuel performance evaluation:

- Fuel Stored Energy
- Fuel Centerline Temperature
- Fuel Temperature Distribution
- Thermal Margins
- Cladding Inner and Outer Surface Temperatures
- Gap Thickness and Conductance Distributions
- Void Volume
- Fission Gas Release Fraction and Composition
- Gas Pressure
- PCI Damage Index
- Oxide Thickness
- Cladding Stress and Strain Distribution
- Axial Growth

A key element of FALCON is the ability to estimate cladding failure by ISCC. Clad failure calculations in FALCON are based on a time-temperature-stress failure criterion fashioned after the cumulative damage concept. Such a concept assumes that the material undergoes cumulative damage due to sustained stress; the higher the stress, the shorter the time to failure. This implies that an applied stress of magnitude σ_0 lasting for a fraction of time Δt will cause the fractional damage ΔD as;

$$\Delta D = \Delta t / t_f(\sigma_0) \qquad (2\text{-}1)$$

where $t_f(\sigma_0)$ is the time to failure had the stress, σ_0, been applied for the total time. Equation (2-1) depends implicitly on the temperature, hence for a given constant temperature T_0, equation (2-1) takes the form

$$\Delta D\,(\sigma_0, T_0) = \Delta t / t_f\,(\sigma_0, T_0) \qquad (2\text{-}2)$$

The relationship for the time to failure used in FALCON has been developed from pressurized Zircaloy tube tests containing iodine gas. These tests provide the time to failure as a function of stress level, temperature, burnup and material type. The expression used in FALCON is [Ref. 5];

$$t_f = \bar{t}\, e^{[0.01015\sigma_y + 0.0174\sigma_{ref} - 0.02755\sigma]} \qquad (2\text{-}3)$$

where

$$\bar{t} = 5 \times 10^5\,(1.13 \times 10^{-4}\,Bu - 0.13)^{-0.75}\ \exp[-30\,(1\text{-}611/T)] \qquad (2\text{-}4)$$

and

σ_{ref}:	$336.476\,(Bu\text{-}5000)^{-0.079262}$	for Zircaloy-2
	$310.275\,(Bu\text{-}5000)^{-0.044}$	for Zircaloy-4
σ_y:	Yield Stress (MPa)	
Bu:	Burnup (MWd/tU)	
T:	Temperature (K)	
σ:	Stress (MPa)	

A threshold stress, σ_{ref}, and a minimum burnup (>5000 MWd/tU) are used in the model and both of these values must be exceeded before SCC is initiated. As shown, the threshold stress decreases as function of burnup and reaches a minimum value near 25 ksi above 20 GWd/tU.

The damage index is calculated in FALCON at each clad element to indicate the potential for cladding failure as a function of time and stress level. The damage index is given by:

$$D = \int_0^{t_n} \frac{dt}{t_f\,(\sigma, Bu, T)} \qquad (2\text{-}5)$$

where D is the amount of damage at t_n, and t_f is the failure time at stress σ, temperature T, and burnup Bu. Damage index values range between zero and 100 in typical PCI analyses.

The above equations and coefficients have been derived primarily from considerable unirradiated and irradiated BWR fuel test data and a limited number of unirradiated and irradiated PWR test data, shown in Figure 2-1 [Ref. 6]. Traditionally in the application to BWR fuel, a value of unity represents the best-estimate measure of cladding failure, i.e., 50% probability of failure, provided the uncertainties have been account for in the analysis. There are too few cases from PWR fuel to develop reliable statistics for a best estimate CDI in PWR cladding. In addition, for application to ZIRLO cladding, it is assumed that the ISCC behavior of ZIRLO is equivalent to Zircaloy-4.

Recommendations for modifying the ramp rate limitations for PWR fuel will be based on relative comparisons of cladding hoop stress and the CDI with that of the baseline case (Zircaloy-4 cladding, threshold of 20%, and a ramp rate of 3%/hr). Considerable operating experience has shown that the potential for PCI failure is extremely low for the current power ramp rate restrictions. Therefore, if the modified ramp rate conditions produce only a small deviation in the cladding stress and CDI from those of the baseline conditions, it can be concluded that the PCI failure potential remains low. This is the basis of the relative comparisons.

For further information on FALCON's fuel rod modeling technique, input requirements, output information, code structure, and calculational procedure, a detailed description is available in the Theory and User's Manuals (Ref. 7, 8) of the FREY code, FALCON's predecessor.

2.3 ESCORE/FALCON Linkage Methodology

The following section describes a passive linkage methodology between the ESCORE or FALCON (r-z model) and FALCON (r-θ) computer codes. The procedure was developed to use ESCORE or FALCON (r-z) as an initialization tool providing steady-state fuel rod irradiation history to FALCON (r-θ) in order to conduct transient fuel rod analyses from a non-zero burnup condition. The philosophy behind the linkage methodology is to initialize the FALCON transient analysis at some non-zero burnup using the results from an ESCORE steady-state analysis. A key requirement of this methodology is to maintain a consistent thermal, mechanical, and material fuel rod state at the linkage point in time. The primary parameters required to convey the irradiation history from the ESCORE steady-state analysis output to the FALCON transient analysis input are the fuel-cladding gap status, cladding permanent strains, and burnup-dependent fuel properties. By using these parameters with FALCON, consistency in the overall fuel rod condition is preserved at the linkage point, minimizing the uncertainties introduced into the transient analysis.

The linkage process is initiated by conducting an ESCORE/FALCON (r-z) full-length (spatial) analysis up to the time and burnup at which the detailed transient analysis is to begin. At the end of the steady-state irradiation period of interest, the power in the ESCORE and FACLON analyses are brought to a hot zero power condition. At this point, the fuel-cladding gap condition, cladding permanent strain state, and the fuel property state are transferred to FALCON (r-θ) using the appropriate output summary tables. Once the information has been input, the FALCON analysis begins with an increase in the linear power to a level matching that used prior to the ramp down in ESCORE. The primary ESCORE or FALCON output data required for linkage are the fuel-clad gap thickness, burnup, fast fluence, fission gas release, internal rod pressure, and cladding strain.

The following is a step by step summary of the procedure used in the linkage methodology between the results of the ESCORE cycle analysis and the FALCON PCI analysis. (FALCON input cards - in bold characters).

Step 1: Conduct ESCORE analysis with the following output summary edits activated:

1) Gap Conductance Summary
2) Detailed Fission Gas Release
3) Rod Pressure – Whole Rod Summary
4) Cladding Dimension Summary

Step 2: Run ESCORE at hot zero power (HZP) conditions.

Step 3: Obtain THERMAL GAP from ESCORE gap conductance summary.

Step 4: Divide THERMAL GAP by as-manufactured radial gap to calculate relative gap thickness. Input on **GAPFAC** set card.

Step 5: Determine COLD ROD PRESSURE and GAP FRACTIONS from rod pressure – whole rod summary. Input on **GAP** command card.

Step 6: Determine rod average fast fluence, rod average actual fuel density, and rod average porosity and input on **NEUTRONICS** and **FUEL** command cards.

Step 7: Determine rod average burnup and input on **CORE** command card.

2.4 General Modeling Approach

The general approach used in this study contains the following main steps:

- Obtain fuel rod dimensions and cladding properties, and develop a full-length fuel rod model.
- Incorporate method (or model) to represent key ZIRLO cladding properties for steady-state analysis of full-length rod with ESCORE and FALCON, and PCI analysis into FALCON.
- Develop cycle power histories for the peak once-burned. Identify the peak nodal power at completion of the startup for the once-burned fuel.
- Develop steady state analysis for once-burned and twice-burned fuel rods using ESCORE and FALCON to establish fuel rod initial conditions for PCI analysis of startup ramp.
- Develop candidate startup ramp conditions (including thresholds and ramp rates).
- Perform PCI analysis using the different startup ramps for both the once-burned fuel rods

2.4.1 Fuel Rod Characteristics and Models

ANATECH worked with Duke Power to develop the fuel rod dimensional and physical characteristics of the fuel pellets and cladding, and the thermal-hydraulic operating conditions of the Westinghouse 17x17 RFA fuel design, which Duke plans to operate in the McGuire and Catawba units. These data, which were obtained from open literature in the public domain, are presented in Table 2-1. Some data were developed on the basis of ANATECH's experience of modeling similar PWR fuel.

The fuel rod design incorporates cladding of an outer diameter of 0.374 inch (9.5 mm) as compared to the 0.360 inch (9.14 mm) diameter of the OFA/V5 fuel design. Both types of cladding have a wall thickness of 0.0225 inch (0.57 mm). Enriched (2.6 w/o U-235) annular pellets comprise the uppermost and lowest 6-inch (152 mm) segments of the fuel stack. The central voids of the blanket regions contribute to the void volume of fuel rod.

The cladding properties are taken from the open literature. The ZIRLO properties are taken from Ref. 8. Special models for growth and creepdown were then developed for modeling ZIRLO in ESCORE and FALCON.

Both codes use different approaches to model the mechanics of the fuel and cladding. ESCORE uses an axial stack of concentric rings in the fuel and the cladding. The ESCORE model is shown in Figure 2-1 with 24 rows and 10 columns (rings), and the cladding is modeled with 24 axial nodes, each representing a separate segment of the cladding. The mechanical behavior of the cladding assumes thin wall tubing. FALCON uses a more sophisticated finite element approach, which enables the use of fewer elements within the fuel. With FALCON, the fuel was modeled with 24 rows and 4 concentric columns of fuel elements, as shown in Figure 2-2. The thermal and mechanical properties are represented with each element by virtue of quadratic shape functions. Each element is comprised of 9 nodes (points of integration), eight on the borders and 1 central to each element. The cladding is modeled as a single column with 24 elements axially oriented.

Table 2-1
Duke Power Design Input for McGuire and Catawba Nuclear Stations

Fuel Parameter	Units English	Value	Units Metric	Value	Reference
Fuel Pellet Parameters					
pellet density	% TD	95.50			FSAR
pellet diameter	inch	0.3225	mm	8.192	FSAR
pellet surface roughness	AA (micro-inch)	32.00	microns	0.81	Typical max clad surface finish
high enriched pellet length	inch	0.3870	mm	9.83	FSAR
blanket pellet length	inch	0.45	mm	10.83	Best Estimate from open literature
blanket length top and bottom	inches	6	mm	150.00	DPC FER letter
blanket pellet inner diameter	inch	0.160	mm	4.064	Estimated from pressure calculations
typical mid stack enrichment	wt %	4.66			DPC FER letter
blanket pellet enrichment	wt %	2.60			Open lit. -
total stack length	inches	144.00	mm	3657.60	FSAR
high enriched pellet dish dia.	inch	0.236	mm	5.99	Tribulation Report & WCAP-11561
high enriched pellet dish depth	inch	0.012	mm	0.30	Tribulation Report & WCAP-11561
high enriched pellet spherical rad.	inch	0.58	mm	14.73	Tribulation Report & WCAP-11561
high enriched pellet chamfer width	inch	0.012	mm	0.30	WCAP-11561, 17x17 OFA
high enriched pellet chamfer length	inch	0.012	mm	0.30	WCAP-11561, 17x17 OFA
high enriched pellet chamfer angle	degrees	45			Derived
grain size	microns	14.0	microns	14.0	Typical ADU UO2 pellet g.s.
Cladding Parameter					
outer diameter	inch	0.374	mm	9.500	FSAR
nominal wall thickness	inch	0.0225	mm	0.572	FSAR
overall length	inches	151.80	mm	3855.72	Fuel Length + Plenum Length
lower plenum length	n/a	n/a	n/a	n/a	n/a
upper plenum length	inches	7.80	mm	198	TVA, Sequoyah UFSAR
ID surface roughness	micro-inch	25.00	micron	0.63	Tribulation Report
Empty plenum volume	cu inch	0.663	cc	10.87	Calculation from clad OD/ID

Table 2-2
Duke Power Design Input for McGuire and Catawba Nuclear Stations

Fuel Parameter	Units English	Value	Units Metric	Value	Reference
Fuel Rod Hardware					
upper end cap length	inch	0.300	mm	7.620	ANATECH Estimate
lower end cap length	inch	0.700	mm	17.780	ANATECH Estimate
plenum spring weight	pounds	0.029	gm	13.15	Estimate from DOE database
plenum spring volume	cu. inch	0.100	cc	1.64	Est. by SS302 @ 0.290#/cu.in
ratio spring vol/empty plen. vol.		0.15			
Fuel Rod Parameters					
Initial Fill Gas Pressure (ADU rod)	psig	275.00	MPa	1.90	Estimate
Estimated Fill Gas Temperature	Degree F	72.00	C	22	Estimate
Rod initially evacuated	n/a	no			n/a
Plenum Spring Rate	lbs/inch	~15-18			ANATECH est.
Plenum Spring Free Length	inches	~9-9.5			ANATECH est.
T/H Boundary Parameters					
Bulk coolant pressure	psi	2250.00	MPa	15.51	DPC Reference
Core mass flow rate	lbm/hr-ft2	2.5826E06			DPC Reference
Core inlet temperature	degree F	554.60	deg. C	290	DPC Reference
Fuel Rod Pitch	inch	0.496	mm	12.60	FSAR
Hydraulic Diameter	inch	0.4635	mm	11.77	Calculation
Cladding Material Properties					
Elastic modulus	Zr-4 / MATPRO				
Poisson's ratio	Zr-4 / MATPRO				
Typical yield strength (RT)	ksi	88	MPa	610	ASTM STP 1245 (Ref. 9)
Typical ultimate strength (RT)	ksi	117	MPa	810	ASTM STP 1245
Estimated dia. creep rate	-	0.8 of Zr-4			ASTM STP 1245
Estimated axial growth rate	-	0.5 of Zr-4			ASTM STP 1245
SCC susceptibility	Zr-4				

2.4.2 ZIRLO Model Development

ANATECH developed a model (method) to represent key ZIRLO cladding mechanical properties in the FALCON fuel behavior code. These key properties included: cladding yield stress, irradiation creep rate, and stress corrosion cracking susceptibility. ANATECH reviewed the available literature data and worked with Duke Power to obtain the information necessary to develop these methods.

PIE data from one and two cycle rods demonstrate that the diametral creep of ZIRLO is approximately 80% of Zr-4 and the irradiation growth is approximately 50% of Zicaloy-4. In the case of ESCORE, two cladding property models were adjusted to represent ZIRLO cladding: diametral creep and irradiation growth. The yield strength was adjusted (decreased) in order to achieve a cladding diametral creep rate of ZIRLO which is approximately 80% that of Zircaloy-4 [Ref. 9]. This approach was selected since the ESCORE cladding creep model consists of two sub-models, one based for irradiation creep and the other for thermal creep. Both creep models are functions of the cladding yield strength [Ref. 10]. The reduced growth of ZIRLO was modeled by applying an appropriate coefficient and exponent for the cladding growth model in the ESCORE input deck.

In the case of FALCON, the creep equation for Zr-4 was modified for ZIRLO by multiplying the creep rate by a coefficient of 0.8. By selecting the variable, MATNDX to be defined as ZIRLO, FALCON selects the ZIRLO creep model, otherwise the user can input the creep rate into the PROP set card associated with the ***CLAD** command card. The cases with ZIRLO cladding were run with a variation of cold-work (cwkf) to model the tendency that ZIRLO has a slightly greater strength than Zr-4.

2.4.3 Establish Fuel Rod Initial Conditions at Startup (Steady-State Fuel Rod Simulation)

Duke Power developed and supplied to ANATECH two power histories for representative once-burned 17x17 RFA fuel in the Catawba 1 unit. One power history is for the peak power fuel rod (Rod E04 in an assembly in core location E-11 in Cycle 13 and core location B11 during Cycle 12) at the beginning of its second cycle (see Figure 2-3). The other power history is for the fuel rod (Rod Q17 in an assembly in core location D12 in Cycle 13 and in core location C-13 during Cycle 12) with the maximum change in power at the beginning of the second cycle (see Figure 2-4). The power history data consisted of fuel rod average power histories (linear powers in kW/ft and radial peaking factors as a function of EFPDs) for one cycle of operation (without coastdown) and the accompanying assembly axial power shapes at core full power conditions. The axial power shapes are provided in Figure 2-5 for period from BOC to 200 EFPD and in Figure 2-6 for the remainder of full power operation during the cycle from 200 to 490 EFPD. Several coastdowns, in conjunction with cycle extension, were introduced to explore the effect of slowly reducing power at end of cycle. The objective of this approach was to obtain a cycle length of at least 490 EFPD while employing an appropriate range of coastdowns. During the coastdown period, the axial power shape at EOC was applied.

During coastdown, the core power is reduced by 1% during a period of 1.5 calendar days (or 0.667%/calendar day). Cycle 12 of Catawba 1 was designed with coastdown of 11% FP (to 89% of core full power), which equates to about 16.5 calendar days. The same power declension rate of 1% per 1.5 calendar days was used in order to model additional coastdowns to 80, 75, and 60% FP in order to determine the fuel-cladding gap behavior over the range of coastdowns possible at Catawba and McGuire.

Using ESCORE and FALCON (in the r-z geometry), ANATECH performed one-cycle steady-state fuel performance analyses based on the power history information. The results of the steady-state analyses were then used to initialize the PCI performance during the startup ramp for the limiting once-burned fuel rod. Similarly, a limited number of twice-burned cases were performed based upon a peak fuel rod power in the third cycle of a twice-burned assembly during the startup.

2.4.4 Power Ramps at Startup (PCI Fuel Rod Simulation)

To evaluate the effects of the threshold power level and the ramp rate on fuel integrity, an analysis matrix consisting of 29 combinations of threshold/ramp rates was developed for use in the evaluation. The analysis matrix used in the evaluation is shown in Table 2-2. The analysis matrix was applied to each reactor and fuel type selected. Current practice of ramp rate restrictions was considered to be a threshold power of 20%FP and a ramp rate 3%FP/hr after the threshold power. This combination of threshold power and ramp rate is referred to as the base case condition. From the matrix of analysis cases, an optimum threshold power level and ramp rate was sought for each fuel and plant type. The ramp rate of 30%/hr is considered the fastest possible uncontrolled (pre-threshold), and is applied to the power transient below the threshold power. The case of "No Threshold" refers to a power ascension from HZP to Full Power with a constant rate of 30%/hr. The entire matrix was applied to cases with Zircaloy-4 cladding. For the cases with ZIRLO cladding, all ramp rates up through 70% were applied since it is unlikely that a greater threshold would be applied.

Table 2-3
Threshold and Ramp Rate Matrix for PCI Analysis

Threshold Power (%FP)	Ramp Rate after Threshold Power (%FP/hr)				
	3	5	10	15	30
20	● (base)	●	●	●	
30	●	●	●	●	
50	●	●	●	●	
60	●	●	●	●	
70	●	●	●	●	
80	●	●	●	●	
90	●	●	●	●	
No Threshold			●	●	●

The fuel rod modeling approach employed in the evaluation used the ESCORE fuel performance program to analyze the one or two cycles of operation prior to the power ramp following a refueling outage. By selecting both once- and twice-burned fuel, an assessment of the impact of burnup was performed. The ESCORE analysis required information describing the fuel rod design, (pellet and clad dimensions, etc.) and the maximum fuel rod power history of each cycle of operation. A full-length axisymmetric (symmetry about the z-axis) analysis was conducted to establish the fuel rod condition at the beginning of the reactor startup power ramp. The parameters of interest were the peak power and burnup location on the fuel rod (axial height), the minimum fuel-cladding gap thickness, rod internal pressure, and fast fluence. These conditions were used to define the axial location that may experience the highest potential for PCI failure (largest cladding stresses).

Once the cycle calculation was performed, the FREY PCI analysis was initiated using the information from ESCORE. The FREY PCI analysis was conducted at the axial slice identified in ESCORE that had the highest potential for PCI failure (i.e. highest burnup and minimum fuel-cladding gap thickness). The FREY analysis was performed using an r-θ representation of the fuel and cladding. Figure 2-7 contains a schematic of the model. The small wedge of the fuel and cladding shown in Figure 2-7 is used to calculate the cladding stress and damage index response during the power change. The PCI model contains a discrete fuel crack as indicated in the figure. This fuel crack establishes stress and strain localization in the cladding once fuel-cladding gap closure occurs during a power ramp. These localized stresses are used to calculate the potential for cladding failure using the cumulative damage model. The cladding hoop stress and damage index results were calculated for each case defined in the analysis matrix. From these results, it was possible to define ramp rate conditions that precluded PCI failure.

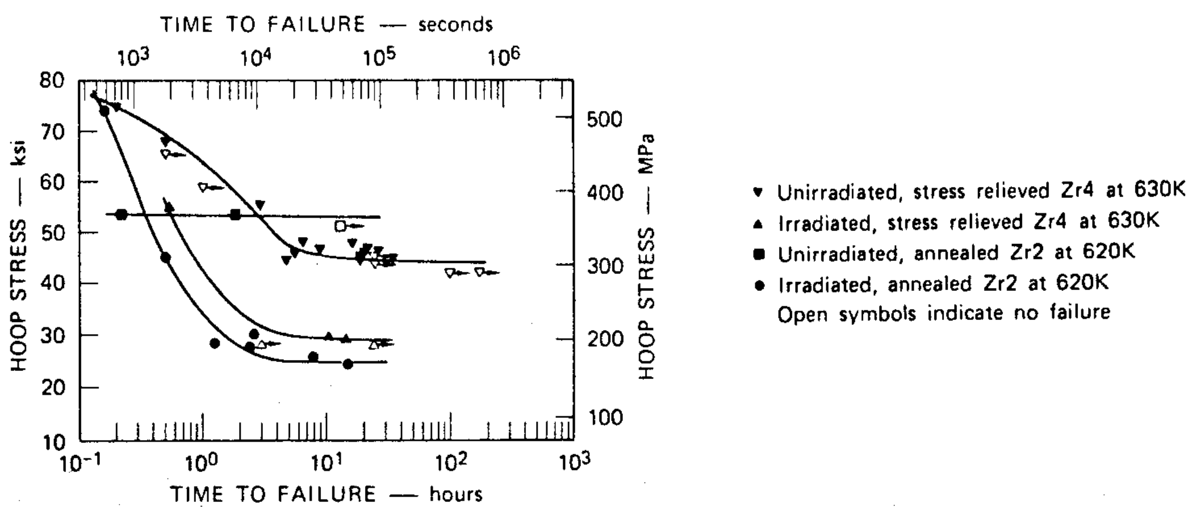

Figure 2-1
Iodine Induced Failure Data for Internally Pressurized Zircaloy Cladding Tubes [Ref. 6]

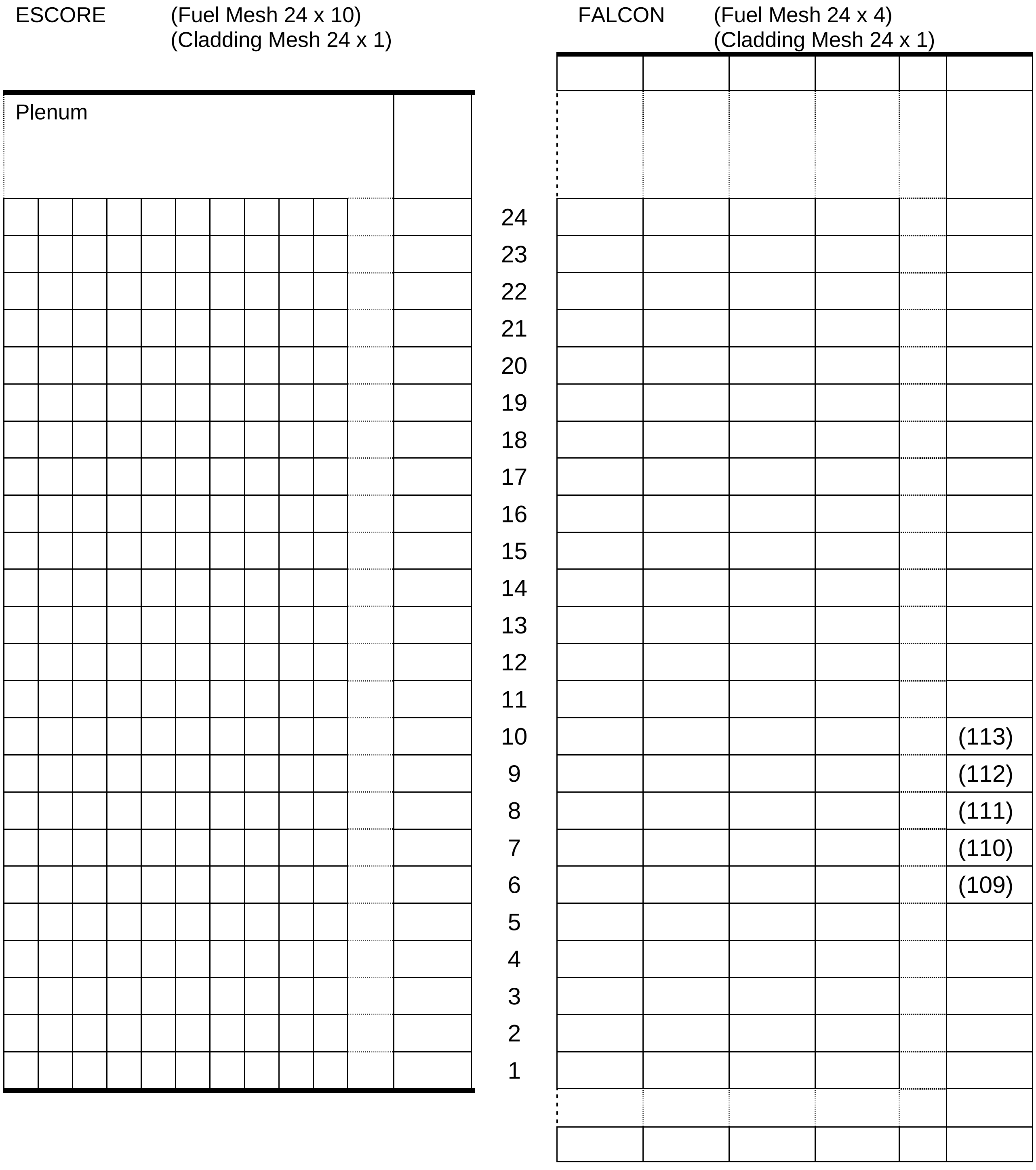

Figure 2-2
Schematics of ESCORE and FALCON Models (Dotted and Dashed Lines are "Gap Elements"). The ESCORE node numbers (1-24) are presented between the models and the FALCON element numbers are presented within parentheses in corresponding elements.

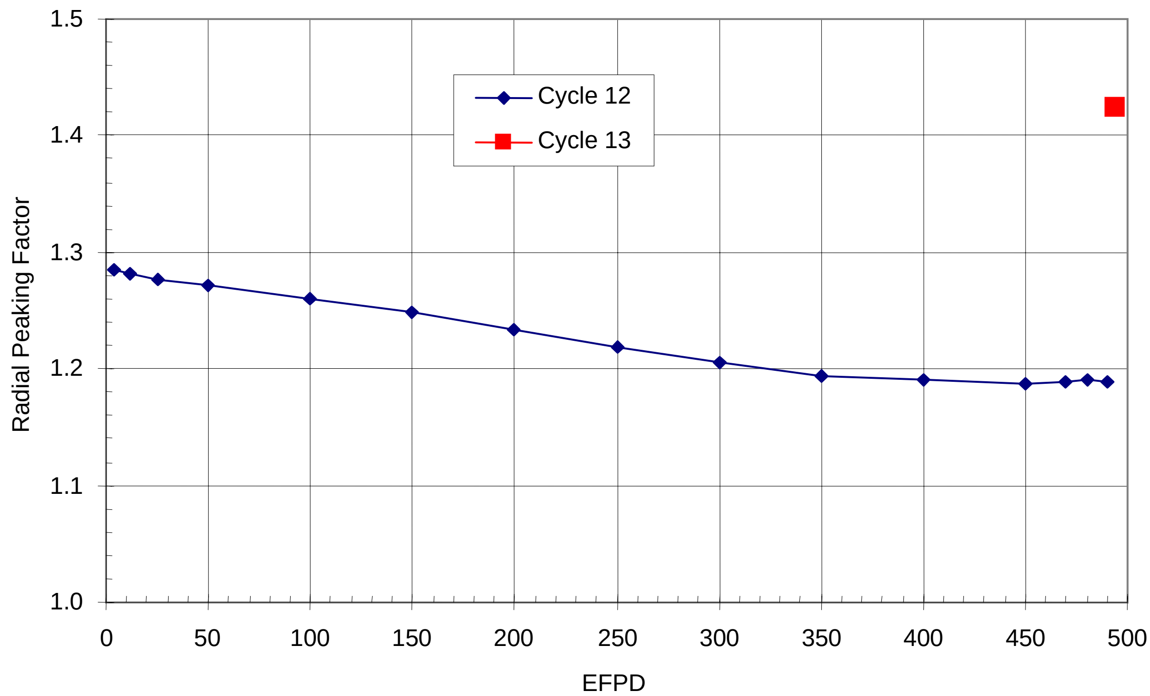

Figure 2-3
Steady-State Power History for Fuel Rod (E04) with the Maximum Power at BOC 2

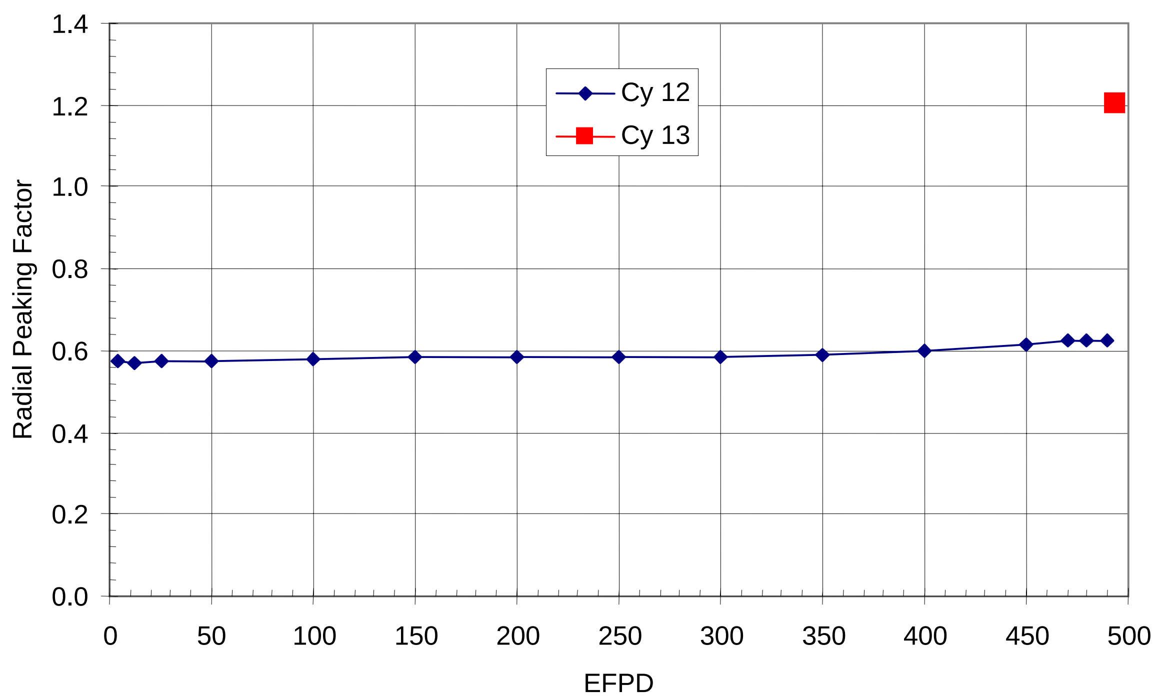

Figure 2-4
Steady-State Power History for Fuel Rod (Q17) with the Maximum Power Increase at BOC2.

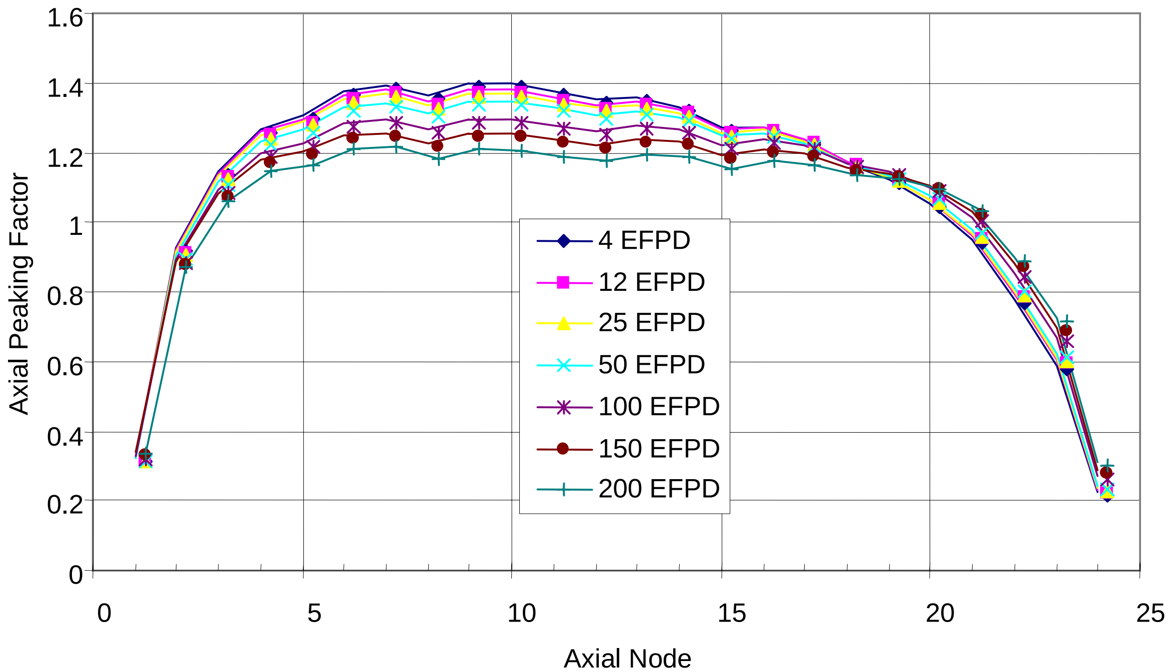

Figure 2-5
Fuel Rod Axial Power Shapes from BOC to MOC (200 EFPD).

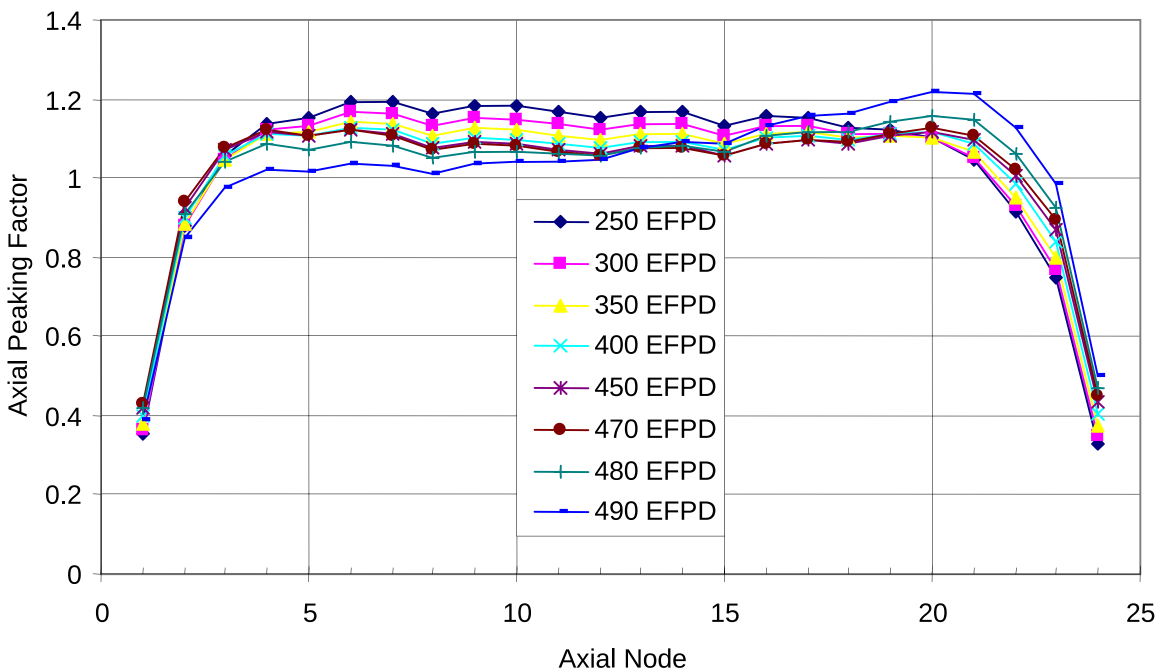

Figure 2-6
Fuel Rod Axial Power Shapes from MOC (200 EFPD) to EOC (490 EFPD)

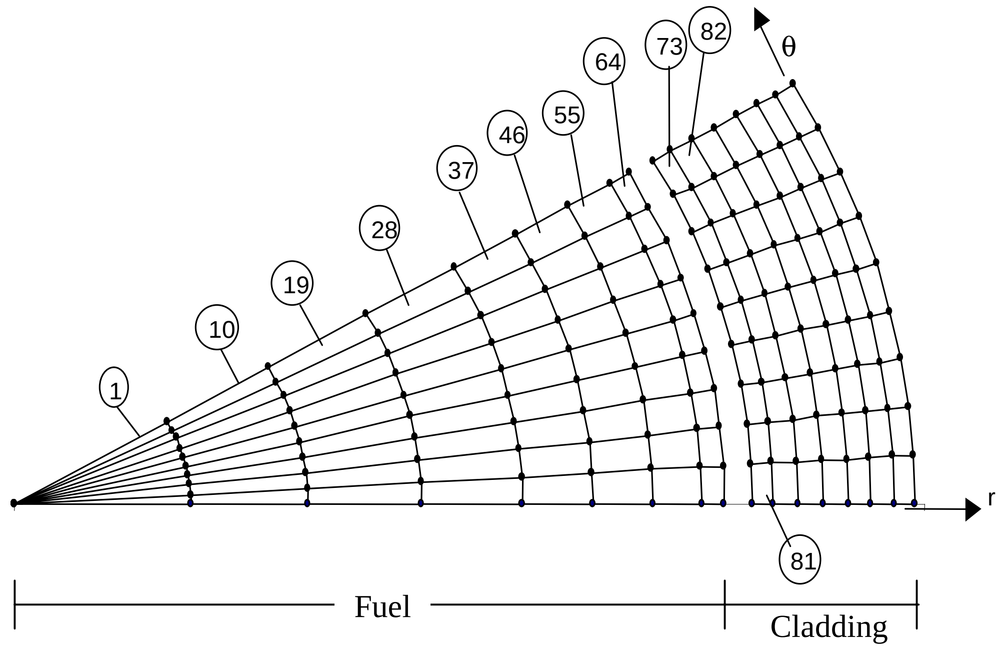

Figure 2-7
FALCON r-θ Library Finite Element Model

3
RESULTS

3.1 Steady-State Analyses

Initial steady-state performance analyses of the two fuel rods (E04 and Q17), discussed in Section 2, were modeled with ESCORE assuming full power operation through the first cycle and into the second cycle. The analyses were repeated with the 89% coastdown beginning at 473.5 EFPD of Cycle 1 and then with a return to full power in the beginning of Cycle 2. The results of the analyses indicated that the cladding of rod Q17 remained in compression at the beginning of the second cycle, while the cladding of E04 experienced tensile stresses.

At the beginning of its second cycle, fuel rod Q17 experiences a peak nodal linear power of 8.22 kW/ft at node 10 (with a local burnup of approximately 12.9 GWD/MTU). The maximum increase in linear power between full power operating levels at end of the first cycle and at the beginning of the second cycle was 5.031 kW/ft. At the node of maximum burnup (13.1 GWD/MTU at node 7), the linear power reached a maximum of 8.07 kW/ft. For ESCORE Nodes 6 through 10, the fuel-cladding (radial) gap remained open with widths in the range of 0.17 to 0.23 mils (4.3 to 5.8 microns). The open gap is the result of the relatively moderate local linear powers (8-8.2 kW/ft) in conjunction with low burnup (13.1 GWD/MTU, peak local burnup, and rod average burnup of 11.54 GWD/MTU). One additional steady-state analysis, with a coastdown to 60% FP, was performed in order to verify that the cladding was still in compression at the beginning of its second cycle.

In the case of fuel rod E04, the rod average burnup at the beginning of the second cycle was approximately 23.65 GWD/MTU with a peak nodal burnup of 26.54 GWD/MTU. This rod had the maximum local linear power at the beginning of the second cycle fuel, with a magnitude of 9.734 kW/ft. The peak local cladding stress predicted by ESCORE was approximately 16.2 ksi at Node 6 (with a burnup of 26.53 GWD/MTU and a local power of 9.56 kW/ft) at the beginning of the second cycle.

Further analyses were performed for fuel rod E04 with several additional coastdowns of 80, 75 and 60%FP. These values span the range of coastdowns projected for the Catawba and McGuire units, and are consistent with practices at other PWRs. A summary of the coastdowns is provided in Table 3-1. For each case, the peak stress, cladding diametral strains, and hot and cold fuel-cladding gaps were compared in order to determine the most limiting case in terms of PCI performance. For Rod E04, only two cases, the coastdowns to 89% and 60%, were analyzed with FALCON. The most limiting or conservative conditions, i.e. the smallest fuel-cladding gap and maximum fission gas inventory in the gap, from both ESCORE and FALCON, were employed in the PCI analyses using FALCON in the R-θ geometry.

Table 3-1
Coastdowns Employed in Steady-State Fuel Rod Power Histories.

End of Coastdown Power Level, % FP	EFPD at Start of Coastdown	EFPD at End of Coastdown	Cycle length Calendar Days
89	473.5	489.1	490
80	490	517.0	520
75	490	522.8	527.5
60	472	520.0	532

The steady-state analyses of Rod E4 were performed for both Zr-4 and ZIRLO cladding. For the steady-state conditions, the diametral creep rate for the ZIRLO cladding was approximately 0.8 that of the Zr-4 cladding, but the fuel-clad gap was approximately the same at corresponding axial locations. This is because the fuel swelling and relocation causes the fuel pellet to intrude into the gap between the fuel and cladding, therefore the difference in cladding creep has little effect on the fuel-clad gap at the moderate burnups of this fuel rod.

The ESCORE predictions of cladding hoop stress in the cladding elements of interest are provided in Table 3-2 for Rod E4 with Zr-4 cladding and in Table 3-3 for Rod E4 with ZIRLO cladding for the startup conditions at the beginning of the second cycle of operation. ESCORE predicts increasing stress as the coastdown continues to lower powers - the highest stresses are predicted for the cases with a coastdown to 60%. In all cases and for both types of cladding, the cold fuel diameter (at cold shutdown conditions) was predicted to be approximately 0.326 inch (8.280 mm) and the cladding inner diameter is 0.327 inch (8.306 mm). These dimensions provided a cold radial fuel-cladding gap of approximately 0.5 mils (12.7 microns). At hot standby (HZP) conditions, the radial fuel-cladding gap was in the range of 0.21-0.25 mils (5.3-6.4 microns).

Table 3-2
Zr-4 Cladding Hoop Stress Predicted by ESCORE at BOC 2 for Rod E04

Coastdown %FP	Cladding Hoop Stress (ksi), ESCORE cladding axial node (corresponding FALCON element no.)				
	6 (Ele 109)	7 (Ele 110)	8 (Ele 111)	9 (Ele 112)	10 (Ele 113)
89	18.053	18.354	18.073	17.522	16.997
80	18.930	18.581	18.191	17.560	16.966
75	19.016	18.687	18.271	17.629	17.027
60	19.118	18.701	18.267	17.620	17.016

Table 3-3
ZIRLO Cladding Hoop Stress Predicted by ESCORE at BOC 2 for Rod E04

Coastdown %FP	Cladding Hoop Stress (ksi), ESCORE cladding axial node (corresponding FALCON element no.)				
	6 (Ele 109)	7 (Ele 110)	8 (Ele 111)	9 (Ele 112)	10 (Ele 113)
89	18.974	18.950	18.607	18.070	17.516
60	19.670	19.120	18.714	18.057	17.415

In conjunction with ESCORE, FALCON was used to model the most limiting case for Rod E4 (Coastdown to 60% FP) with both Zr-4 cladding and ZIRLO cladding. The results of the predicted cladding stresses are shown in Table 3-4. Both codes predict that ZIRLO will have slightly higher stress at the same power level than Zircaloy-4. The codes differ with respect to which node has the maximum stress - ESCORE predicts the maximum stress in Node 6 (corresponding to FALCON Element 109) and FALCON predicts the maximum stress in Element 113 (corresponding to ESCORE Node 10). Node 6 (Ele 109) corresponds to the location of maximum burnup in the fuel rod E04, whereas Node 10 (Ele 113) corresponds to the peak power location at the beginning of the second cycle. For the development of the PCI model the maximum burnup condition and the peak nodal power were applied, thus providing the most conservative combination.

Table 3-4
Comparison of Zr-4 and ZIRLO Cladding Stresses Predicted by ESCORE and FALCON for the Rod E4 with Coastdown to 60%FP

Zircaloy - 4					ZIRLO (YS(ZIRLO)=YS(Zr-4))				
ESCORE		FALCON			ESCORE		FALCON		
Node	Stress (ksi)	Ele	Peak Stress (ksi)	144 hrs Stress (ksi)	Node	Stress (ksi)	Ele	Peak Stress (ksi)	144 hrs Stress (ksi)
6	19.118	109	42.383	17.045	6	19.670	109	43.80	18.212
7	18.701	110	44.129	17.168	7	19.120	110	45.672	18.615
8	18.267	111	44.899	17.243	8	18.714	111	46.456	18.452
9	17.620	112	45.630	17.343	9	18.057	112	47.311	19.093
10	17.016	113	45.90	17.326	10	17.415	113	47.606	19.284

It should be emphasized that ESCORE is a strictly steady-state thermo-mechanical modeling code and therefore does not provide the peak stresses predicted by FALCON. FALCON, with its transient capability predicts high stresses in conjunction with power changes, then allows the fuel and cladding to relax, which then reduces the local stress. In the FALCON cases, the power change from HZP to FP at BOC2 was performed with a ramp rate of 10%/hr. The differences between the codes regarding the predicted stress levels reflect the differences in models and capabilities of both codes.

3.2 Startup Power Ramp (PCI) Analyses

For the PCI cases, fuel dimensional data, local fuel conditions as a function of burnup were incorporated into the FALCON R-θ PCI model as discussed in Section 2. The following principal cold (pool temperatures) dimensions were used:

Fuel Pellet Outer Diameter (FUELOD)	=	0.326 inch (increase of 3.5 mils from 0.3225 inch at BOL)
Cladding Inner Diameter (CLADID)	=	0.327 inch (decrease of 2 mils from 0.329 inch at BOL)
Cladding Outer Diameter (CLADOD)	=	0.371 inch (decrease of 3 mils from 0.374 inch at BOL)

These dimensions correspond to the fuel pellet and cladding dimensions for Rod E04 at the cold conditions after a coastdown to 60% FP, and provide a cold radial gap of 0.5 mils (12.7 microns). This would then provide a hot (HZP) radial gap of approximately 0.25 mil (6.3 microns). To add to the conservatism of the PCI analyses, the fuel-cladding gap at cold conditions is reduced by a factor of 0.5 (**GAPFAC = 0.5**). As a result of this approach, FALCON predicts a closed gap at HZP conditions for the PCI analysis.

The local irradiation conditions included a burnup of 26.3 GWD/MTU and a fast fluence (E > 1 MeV) of approximately 5.1 E+21 n/cm^2. Other parameters such as fuel rod internal pressure, local (bulk) coolant temperature, and film (heat transfer) coefficient were input as functions of time and power. These data and the fission gas composition were taken from the values calculated by FALCON (in the r-z mode) at elevation corresponding to Node 10 of ESCORE (Node 10 of 24, in which Node 1 is the bottom 6-inch node of the fuel stack) as shown in Figure 2-2.

The set of startup ramp conditions (ramp rates and threshold power levels, shown in Table 2-2) used in the PCI analyses were provided by Duke Power based on the current operating practices. A total of 4 different "restricted" ramp rates (3%/hr, 5%/hr, 10%/hr and 15%/hr) were selected for each threshold, and a fifth ramp rate (30%/hr, considered to be the fastest possible "unrestricted" power ramp rate) was applied up to each threshold. The complete set of ramp conditions was applied to Rod E4 with Zircaloy-4 cladding. This approach established a baseline with which to compare the predictions with ZIRLO cladding and also enabled a comparison with previous work to assure that the methodology and results were consistent with the previous work.

For the cases with ZIRLO cladding, a reduced set of ramp conditions was employed: the no-threshold case and those cases with thresholds of 20%, 30% and 50%FP with the four restricted ramp rates (3, 5, 10 and 15%/hr) were analyzed. For the thresholds of 60% and 70% FP, the analyses were performed only for the "restricted" ramp rate of 5%/hr. This limited set provides a good comparison to the Zircaloy-4 matrix. Furthermore, the cases of most interest are those with the 60% threshold (the most likely maximum threshold of interest by Duke) and the 70% threshold (to provide some idea of margin beyond the 60% threshold), both at the post-threshold ramp rate of 5%/hr.

In additions to the cases just mentioned, a set of sensitivity analyses were conducted for the ramp condition of most interest, namely with thresholds of 60% FP and 70% FP, and both with a ramp rate of 5%/hr. The five sets included:

- Ramping the fuel to a peak nodal power of 10.22 kW/ft, which corresponds to 105% of the base peak nodal power (9.734 kW/ft) provided by Duke for Rod E04 at BOC 2,
- Adding an oxide layer and reducing the wall thickness correspondingly and ramping to the base local power or 9.734 kW/ft,
- A combination of the ramping to 105% of the base power with the reduced cladding wall thickness,
- And ramping to the base peak local power of 9.734 kW/ft at a higher local burnup (28.0 GWD/MTU which is 106.4% of the base local, and
- An assessment of twice-burned fuel with a coastdown of 60% during the second cycle and a ramp to a power level consistent with a peak pin radial power factor of 1.089.

The results of these analyses are presented in the following sections. All peaking factors are based on a core average linear power of 5.58 kW/ft and normalized axial power factors with respect to the rod average power.

3.2.1 Results of PCI Analyses of Rod E04 with Zircaloy-4 Cladding

For all of the cases, in which a threshold is imposed, an "unrestricted" ramp rate of 30%/hr is imposed below the threshold. At full core power (FP), the maximum peak nodal power is assumed to be 9.734 kW/ft. The peak cladding hoop stress and cladding cumulative damage index (CDI) predicted by FALCON from the PCI analyses for once-burned Rod E04 with Zircaloy-4 cladding are summarized in Table 3-5. The same data are graphically represented in Figures 3-1 through 3-4 in which the peak cladding stress and CDI are plotted parametrically as functions of post-threshold ramp rate (%/hr) and threshold power level (%FP).

The data show that for the range of thresholds from 20%FP (the base or reference threshold, which corresponds to a nodal linear power of 1.947 kW/ft) up to 70%FP, the peak hoop stress and CDI are relatively independent (constant) of the threshold, for ramp rates of 5%/hr or less.

Under the conditions of a threshold of 70%FP (6.8 kW/ft) with a ramp rate of 3%/hr (0.292 kW/ft/hr) to FP (9.734 kW/ft), the peak stress is approximately 43.8 ksi and the CDI is 0.303. For the same threshold, but with an increase in the post-threshold ramp rate to 5%/hr (0.487 kW/ft/hr), the peak stress increases slightly to 48.5 ksi and the CDI increases to a value of 0.457. This cladding hoop stress and CDI values are comparable to those for the conditions of 60% threshold (5.84 kW/ft) with a restricted ramp rate of 5%/hr.

Table 3-5
Peak Cladding Stress and Cumulative Damage Index (CDI) Predicted by FALCON for 17x17 RFA Rod E04 with Zircaloy-4 Cladding for Various Startup Regimes

Threshold % FP	Ramp Rate							
	3%/hr		5%/hr		10%/hr		15%/hr	
	Stress (ksi)	CDI	Stress (ksi)	CDI	Stress (ksi)	CDI	Stress (ksi)	CDI
20	43.671	0.2962	48.240	0.4338	54.534	0.7203	57.957	0.9257
30	43.569	0.2832	48.225	0.4320	54.534	0.7197	58.015	0.9614
50	43.671	0.2942	48.196	0.4302	54.534	0.7221	58.030	0.9553
60	43.656	0.2948	48.254	0.4534	54.607	0.7270	58.030	0.9347
70	43.772	0.3030	48.457	0.4571	54.810	0.7480	58.233	0.9810
80	45.440	0.3823	49.211	0.5328	55.433	0.8270	58.682	1.0451
90	54.694	0.6126	54.694	0.7868	57.203	1.0183	59.814	1.1639

Beyond a threshold of 70%, the peak cladding hoop stress and CDI begin to increase significantly due to the fact that the fuel and cladding cannot relax faster than the loading (and strain rate) imposed by the thermal expansion of the fuel. In addition, the peak cladding hoop stress and CDI for the cases of the higher ramps rates of 10% and 15%/hr are significantly greater than those at the lower ramp rates of 3 and 5%/hr. These data indicate that a limit of 5% is a practical upper limit for the restricted ramp rate.

In order to provide a better understanding of the significance of the threshold, several analyses were performed without a threshold; i.e. the same ramp rate was used from HZP to FP conditions. The results, which are provided in Table 3-6, show an important relationship involving the threshold, and the ramp rates before and after the threshold. For example, for the 10%/hr ramp rate without a threshold, the peak cladding hoop stress (54.578 ksi) and CDI (0.728) are approximately equal to respective values for the cases for which the thresholds were 60% and 70% with a post-threshold ramp rate of 10%/hr. Similarly, for the case with a ramp rate of 15%/hr without a threshold, the peak cladding hoop stress (58.044 ksi) and CDI (0.9582) are approximately equal to respective values for the cases for which the thresholds were 60% and 70% with a post-threshold ramp rate of 15%/hr. In the cases with the thresholds, for which the data a provided in Table 3-5, the pre-threshold, or "unrestricted" ramp rate was 30%/hr. Therefore, these results indicate that the peak cladding hoop stress and CDI are virtually independent of the ramp rate below the threshold of approximately 70%FP, or a local linear power of 6.8 kW/ft. In addition, imposing a threshold of 60% will provide some additional margin.

Table 3-6
Peak Cladding Stress and Cumulative Damage Index Predicted by FALCON for 17x17 RFA Rod E04 with Zircaloy-4 Cladding for Various Continuous Ramps Without a Threshold

Ramp Rate							
10%/hr (0.973 kW/ft/hr)		15%/hr (1.460 kW/ft/hr)		20%/hr (1.947 kW/ft/hr)		30%/hr (2.92 kW/ft/hr)	
Stress (ksi)	CDI	Stress (ksi)	CDI	Stress (ksi)	CDI	Stress (ksi)	CDI
54.578	0.728	58.044	0.9582	60.321	1.1494	63.178	1.4252

In order to provide a better definition of the value of the linear power, which corresponds to a suitable threshold, several cases were run in which the power was ramped at a rate of 30%/hr to several power levels (6.035, 6.619, 7.008, 7.592, 7.891 and 8.498 kW/ft), and then the power was held constant. The results are provided in Table 3-7 and graphically in Figures 3-5, 3-6 and 3-7. The data show that, for fast ramp rates (e.g. 30%/hr or 2.92 kW/ft/hr), the damage incurred by the cladding during the ramp is not as severe as the damage incurred after the terminal power is achieved, at least for power levels less than approximately 8 kW/ft. At the linear power of 8.5 kW/ft, the CDI begins to increases at a more significant rate.

Table 3-7
Peak Cladding Hoop Stress and CDI for Various Constant Local Power Levels Following a Ramp from HZP at a Rate of 30%/hr (2.92 kW/ft/hr)

Ramp Terminal Power (kW/ft)	%FP	Peak Stress (ksi)	CDI (-)
6.035	62.0%	28.688	0.00375
6.619	68.0	34.127	0.00480
7.008	72.0	37.855	0.0124
7.592	78.0	43.457	0.0389
7.921	81.4	46.514	0.0660
8.492	87.2	52.025	0.1898

All of the CDI shown in Table 3-7 are considerably less than the CDI's shown in the other tables, where the ultimate power level went to 100% or 9.734 kW/ft. In particular, the CDI values for the power less than or equal to 7.6 kW/ft (78.0 %FP) are very low, less that 0.04, as compared to a value of 0.5, the benchmark value for this study. Significantly more margin is obtained with a threshold of 60% FP (5.8 kW/ft), which is below the lowest value in the table.

Finally, the results of the cases of particular interest 60_05 (60% threshold, 5%/hr ramp rate) and 70_05 (70% threshold, 5%/hr ramp rate) are compared to the base case 20_03 (20% threshold, 3%/hr ramp rate) and to two cases without a threshold at power ascension rates of 15%/hr and 30%/hr. The nodal power histories are provided in Figure 3-8 and the cladding hoop stress and CDI are provided in Figures 3-9 and 3-10 respectively. The peak stress for cases 60_05 and 70_05 are 48.25 and 48.48 ksi, respectively, and represent an increase of 11% over the base case. The corresponding CDI are 0.4354 and 0.4571, which represent increases of 48% and 55% above the CDI (0.2942) of the base case. However, both CDI's are less the 1.0, the benchmark value. In contrast the no threshold cases, with ramp rates of 15% and 30%/hr cause a significant increase in stress and CDI.

3.2.2 Results of PCI Analyses of Rod E04 with ZIRLO Cladding

The results for the PCI analysis of Rod E04 with ZIRLO cladding are summarized in Table 3-7 and are graphically represented in Figures 3-11 through 3-14. As one would expect, ZIRLO cladding, with its higher creep resistance (reduced creep) than Zr-4 cladding, experiences higher levels of stress and greater CDI values than those of Zr-4 cladding under corresponding power ramp conditions. For these analyses, ANATECH assumed that the yield strength of ZIRLO is equivalent to that of Zr-4 at the same fluence level (both materials had the cold work factor, cwkf = 0.1, in the FALCON model).

Table 3-8
Peak Cladding Stress and Cumulative Damage Index (CDI) Predicted by FALCON for 17x17 RFA Rod E04 with ZIRLO Cladding for Various Startup Regimes

Threshold % FP	Ramp Rate							
	3%/hr		5%/hr		10%/hr		15%/hr	
	Stress (ksi)	CDI	Stress (ksi)	CDI	Stress (ksi)	CDI	Stress (ksi)	CDI
20	45.749	0.4439	50.343	0.6162	56.449	1.0421	59.770	1.3585
30	45.730	0.4410	50.299	0.6449	56.449	1.0423	59.741	1.3702
50	45.716	0.4546	50.314	0.6617	56.492	1.0780	59.814	1.4103
60	-	-	50.372	0.6685	-	-	-	-
70	-	-	50.589	0.6925	-	-	-	-

One additional case with no threshold and a ramp rate of 30%/hr produced a peak stress of 64.571 ksi and the CDI of 2.0181. The hoop stress for the ZIRLO cladding is only slightly higher than the value of 63.178 calculated for Zr-4, but the CDI for ZIRLO is approximately 30% greater than the value of 1.4252 calculated for Zr-4. The slightly higher peak stress and greater CDI are directly a consequence of modeling ZIRLO with a total (irradiation and thermal) creep rate of 80% that of Zircaloy-4. In actuality, ZIRLO is believed to have a somewhat higher thermal creep rate, in which case the cladding relaxation would be actually closer to that of Zircaloy-4, and therefore the peak stresses and CDI may be approximately those for Zircaloy-4.

ZIRLO cladding is slightly stronger than Zr-4 cladding for the same metallurgical condition and this relationship is preserved somewhat during irradiation. Therefore, a limited parametric study was performed for three different levels of cold work factor (cwkf = 0.10, 0.20 and 0.25), and therefore three levels of yield strength, for the two power ascension regimes of most interest. The results, provided in Table 3-8, show that as the cold work increases, the peak hoop stress does not change (decrease) significantly, but the CDI, a function of yield strength (and implicitly cold work) does decrease. For a cold work factor of 0.25, the yield strength of ZIRLO is approximately 5.2 ksi greater than that of Zr-4 at HZP conditions (557°F / 292°C) and approximately 3.7 ksi greater than that of Zr-4 at HFP conditions (711°F / 377°C).

Table 3-9
Peak Hoop Stress and CDI for ZIRLO Cladding as a Function of Cold Work

Case	Cold Work Ratio					
	cwkf =0.10 YS(HZP)=93.1 ksi YS(HFP)=80.0 ksi		cwkf =0.20 YS(HZP)=96.6 ksi YS(HFP)=82.5 ksi		cwkf =0.25 YS(HZP)=98.3 ksi YS(HFP)=83.7 ksi	
	Stress (ksi)	CDI	Stress (ksi)	CDI	Stress (ksi)	CDI
60_05	50.372	0.6685	49.922	0.5187	49.675	0.4563
70_05	50.589	0.6925	50.140	0.5408	49.893	0.4798

When comparing the data for these two cases with the corresponding data in Table 3-5, one observes that if ZIRLO has a higher yield strength at HFP (YS = 83.7 ksi, equivalent to cwkf = 0.25 in FALCON) than Zr-4, then the higher yield strength contributes to a lower CDI. In other words, higher yield strength will compensate for the effects of increased creep resistance. Therefore, if ZIRLO cladding has greater yield strength than Zr-4 cladding, the results for Zr-4 presented in Table 3-5 could be considered valid for ZIRLO.

3.2.3 Results of Additional Sensitivity Studies

3.2.3.1 Ramp to 105% of Reference Linear Power at BOC 2.

In order to assess the suitability of these analyses to other power conditions, the PCI behavior of Rod E04 with Zr-4 and ZIRLO cladding was analyzed up to a full power peak nodal linear heat rate of 10.22 kW/ft. This higher linear power corresponds to a factor of 1.05 times the peak nominal maximum linear heat rate of 9.734 kW/ft provided by Duke Power, and could be representative of the fuel operating with a 5% uprate of the plant. The peak cladding stress and CDI are provided in Table 3-9.

Table 3-10
Peak Hoop Stress and CDI for Rod E4 Ramped to 10.22 kW/ft (105% of the Reference LHGR (9.734 kW/ft))

	Zr-4		ZIRLO			
			(cwkf = 0.25)		(cwkf = 0.20)	
Power Ascension	Peak Stress (ksi)	CDI (-)	Peak Stress (ksi)	CDI (-)	Peak Stress (ksi)	CDI (-)
60_05	50.314	0.7690	51.067	0.8253	52.214	0.9292
70_05	50.531	0.7896	52.214	0.8597	52.417	0.9724

The magnitudes of the stresses and CDI for the Zr-4 cladding are comparable to those in Table 3-5 for the cases with a ramp rate of 10%/hr. The ZIRLO shows slightly higher stresses, but the CDI are at least 7% greater for ZIRLO with a cold work factor of 0.25. For the ZIRLO with a cold work factor of 0.2, the CDI are at least 20% greater than those of Zr-4 cladding. These levels of stress and CDI indicate a strong PCI interaction.

3.2.3.2 Ramp to Reference Linear Power with Reduced Cladding Wall Thickness

Oxidation of the cladding results in a loss of wall thickness. In order to assess the sensitivity of the calculations to the wall thickness, selected cases were reanalyzed with an additional reduction in wall thickness. The cladding wall thickness was reduced by 2 mils for the Zr-4 cladding and only 1 mil for the ZIRLO cladding. The stresses and CDI values are provided in Table 3-10.

The magnitudes of stress and CDI in Table 3-10 for the Zr-4 cladding and ZIRLO cladding are approximately equal to those in Tables 3-5 (Zr-4) and 3-8 (ZIRLO) for the same power ascension conditions. Therefore, the loss of wall thickness assumed for these analyses did not have a significant effect on the peak cladding stress or CDI.

Table 3-11
Peak Hoop Stress and CDI for Rod E4 Ramped to the Reference LHGR (9.734 kW/ft) with Reduced Wall Thickness of the Cladding

	Zr-4		ZIRLO			
			(cwkf = 0.25)		(cwkf = 0.20)	
Power Ascension	Peak Stress (ksi)	CDI (-)	Peak Stress (ksi)	CDI (-)	Peak Stress (ksi)	CDI (-)
60_05	48.457	0.4233	49.762	0.4472	50.023	0.5078
70_05	48.675	0.4366	50.009	0.4673	50.256	0.5325

3.2.3.3 Ramp to 105% of Reference Linear Power with a Reduced Cladding Wall Thickness

Both increased peak nodal power and wall thinning were evaluated together. The magnitudes of the stresses and CDI are approximately those given in Table 3-9, at the higher linear power, but without wall thinning. These results indicate that the nodal power is the more significant factor with respect to the PCI performance.

Table 3-12
Peak Hoop Stress and CDI for Rod E4 Ramped to 10.22 kW/ft (105% of the Reference LHGR (9.734 kW/ft)) with Reduced Wall Thickness of the Cladding

	Zr-4		ZIRLO			
			(cwkf = 0.25)		(cwkf = 0.20)	
Power Ascension	Peak Stress (ksi)	CDI (-)	Peak Stress (ksi)	CDI (-)	Peak Stress (ksi)	CDI (-)
60_05	50.560	0.7349	52.192	0.8680	52.330	0.9257
70_05	50.749	0.7789	52.344	0.8621	52.547	0.9647

3.2.3.4 Ramp to Reference Linear Power at a Local Burnup of 28 GWD/MTU

The nominal peak nodal burnup for the 17x17 RFA in Catawba fuel was approximately 26.3 GWD/MTU. With a cycle extended to approximately 525 EFPD, the peak nodal burnup in Rod E04 approaches 28.0 GWD/MTU. Therefore, it was decided to perform a limited analysis with

Zr-4 and ZIRLO (with a cold-work factor of 0.25), for only one power ascension, 60_05, for the two maximum nodal linear power of 9.734 and 10.22 kW/ft. The results, provided in Table 3-12, are consistent with the data presented in the previous tables. The PCI performance is acceptable for the case of 9.734 kW/ft, but strong PCI interaction is indicated for the higher linear power of 10.22 kW/ft.

Table 3-13
Peak Hoop Stress and CDI for Rod E4 Ramped to 9.734 and 10.22 kW/ft at a Local Burnup of 28 GWD/MTU

Terminal Power (kW/ft)	Zr-4		ZIRLO (cwkf = 0.25)	
	Peak Stress (ksi)	CDI (-)	Peak Stress (ksi)	CDI (-)
9.734	48.501	0.4636	49.965	0.4895
10.22	50.560	0.8128	52.257	0.8796

3.2.3.5 PCI Analyses of Twice-Burned Fuel

The analysis of twice-burned fuel is slightly more complicated than once-burned fuel because the condition of the fuel and cladding is not only determined by the actual burnup of the fuel, but also by the power history involved. The variation of power histories and accumulated burnups in twice-burned fuel is considerably greater than for once-burned fuel.

The analyses for twice-burned fuel were limited to a single cladding node with a local exposure of 42.5 GWD/MTU and a single power ascension of 5%/hr after a threshold of 60%. However, several nodal powers from the mostly likely nominal power (7.6 kW/ft) up to the reference linear power (9.734 kW/ft) for once-burned fuel were analyzed. Table 3-13 provides the set of linear powers and related peaking factors.

Table 3-14
Linear Power and Peaking Factors for PCI Analysis of Twice-Burned 17x17 RFA Fuel with a Nodal Exposure of 42.5 GWD/MTU.

Nodal lhgr (kW/ft)	Pkf (node/core avg lhgr)	Max. axial pkf Peak node Pkf / Max rod radial pkf	Max Pin Radial Peaking Factor (Local Pkf / Max axial pkf)	
	lhgr/5.58	Pkf / 1.089	Pkf/1.225	Pkf/1.245
7.6	1.362	1.2507	1.1118	1.0940
8.0	1.434	1.3165	1.1704	1.1516
8.5	1.523	1.3988	1.2435	1.2235
9.0	1.613	1.4811	1.3167	1.2955
9.734	1.744	1.6019	1.4240	1.4012

The results of the analyses are given in Table 3-14 for Zr-4 and ZIRLO claddings. Below a linear power of 9 kW/ft, both types of cladding show moderate local stresses and low CDI values as compared to the peak power once-burned fuel.

Table 3-15
Peak Stress and CDI for Twice-Burned 17x17 RFA Fuel with a Nodal Exposure of 42.5 GWD/MTU.

Cladding		Linear Power				
		7.6 kW/ft	8.0 kW/ft	8.5 kW/ft	9.0 kW/ft	9.734 kW/ft
Zr-4	Peak Stress (ksi)	37.434	39.842	42.627	45.410	48.588
	CDI (-)	0.0391	0.0701	0.1325	0.2384	0.525
ZIRLO	Peak Stress (ksi)	37.681	40.320	43.353	46.354	50.023
	CDI (-)	0.0359	0.0644	0.1266	0.238	0.5346

Based on data provided by Duke Power for Catawba 1, Cycle 13, which included fuel assembly burnups, and assembly and peak rod peaking factors at BOC, the center assembly in the core should have the maximum local peaking for twice-burned (or possibly thrice-burned) fuel. For this analysis, it was assumed that the assembly peaking factors applied to a twice-burned assembly with a burnup of approximately 36.1 GWD/MTU with a peak pin exposure of 37.8 GWD/MTU. Based on data supplied by Duke Energy, the maximum local nodal exposure was estimated to be approximately 42.5 GWD/MTU, which represents an average local exposure peaking factor of 1.12 (axial node/fuel rod). Applying the maximum axial peaking factors from Rod E04 as once-burned (1.225) and as fresh fuel (1.245), the peak nodal power of the center assembly in Catawba is likely to be less than 7.6 kW/ft, as shown in Table 3-15. A threshold of 60% would correspond to a local linear power of 4.56 kW/ft, and change of approximately 3 kW/ft to full power. This is not a significant power change, especially when considering the low CDI values shown in Figure 3-7 and Table 3-14. Therefore, this fuel is not limiting with regard to a threshold of 60% and a power ascension rate of 5%/hr, at a local burnup of 42.5 GWD/MTU. The data in Table 3-14 also show substantial margin at this power level.

Table 3-16
Most Probable Peak Nodal Linear Powers for Third Cycle Fuel

LHGR (kW/ft)	Most Likely* Radial Pkf	Max Axial Pkf	Core Avg LHGR (kW/ft)
7.444	1.089	1.225 (Max. axial pkf for once burned fuel)	5.58
7.565		1.245 (Max. axial pkf for fresh fuel)	
* CNC-1553.05-00-0327, Rev 2, Corr 2 CNEI-0400-29, Rev. 11			

3.3 Assessment of the Threshold for 17x17 RFA Fuel Rod with ZIRLO Cladding

Duke Power plans to use Westinghouse 17x17 fuel in the Catawba and McGuire units and this fuel will be manufactured with ZIRLO cladding. The objective of these analyses has been to determine if the fuel could be operated during the plant startup with a threshold of 60%FP followed by a ramp rate of 5%/hr. Previous work by ANATECH and EPRI has demonstrated that Zr-4 cladding could operate under such conditions.

For this project, the Westinghouse 17x17 RFA fuel rod design using both Zr-4 and ZIRLO claddings was analyzed for a variety of conditions during startup at the beginning of a second and third cycle. The results indicate that the ZIRLO cladding can operate under conditions similar to Zr-4 cladding, provided that ZIRLO has slightly greater yield strength than Zr-4. The higher yield strength of ZIRLO compensates for the slightly greater creep resistance. If ZIRLO is fabricated, such that the yield strength is approximately that of Zr-4, then the ramp rate should be limited to 3%/hr, although 4%/hr may be possible. On the other hand, the modeling of ZIRLO cladding was conservative in the sense that the total creep rate was modeled as 80% that of Zircaloy-4. This approach consequently lead to higher predicted stresses. It is apparent that ZIRLO may actually have a higher thermal creep rate than was used in this study. In this case, ZIRLO performance would be more like that of Zircaloy-4.

These analyses also show that Zr-4 and ZIRLO can be operated with a threshold of 60%FP and a subsequent power ascension to full power at 5%/hr with margin to PCI. The threshold of 60%FP is equivalent to a local nodal power of 5.8 kW/ft, based on a peak nodal power of 9.734 kW/ft, and the ramp rate of 5%/hr is equivalent to a linear power rate increase of 0.487 kW/ft/hr. If the nodal linear power is greater at full power conditions, then the threshold or ramp rate should be reduced.

The threshold in terms of %FP and ramp rate in terms of %FP/hr is actually a function of the peak nodal power at full power. These relationship are illustrated in Figure 3-13 which provides the threshold and ramp rate as functions of local (nodal) linear power at the full power condition. These could be translated to assembly radial power if the appropriate bounding peaking factors are known.

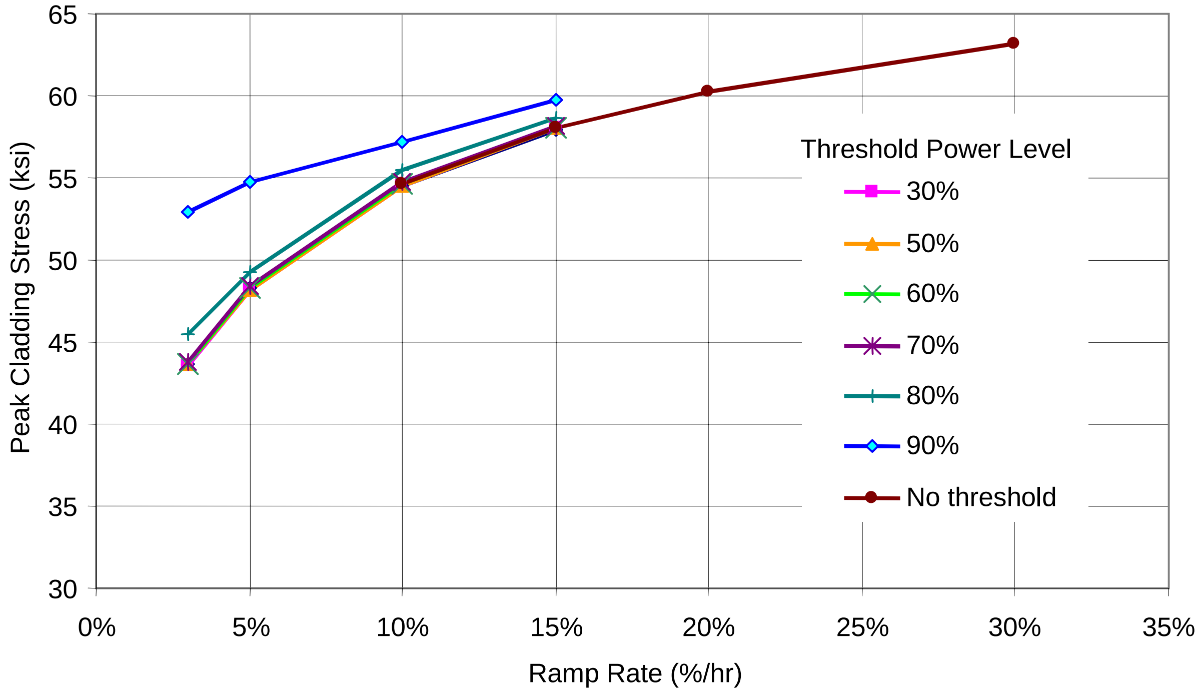

Figure 3-1
Peak Cladding Hoop Stress as a Function of Post-Threshold Ramp Rate of Zr-4 Cladding (Pre-threshold Ramp Rate = 30%/hr)

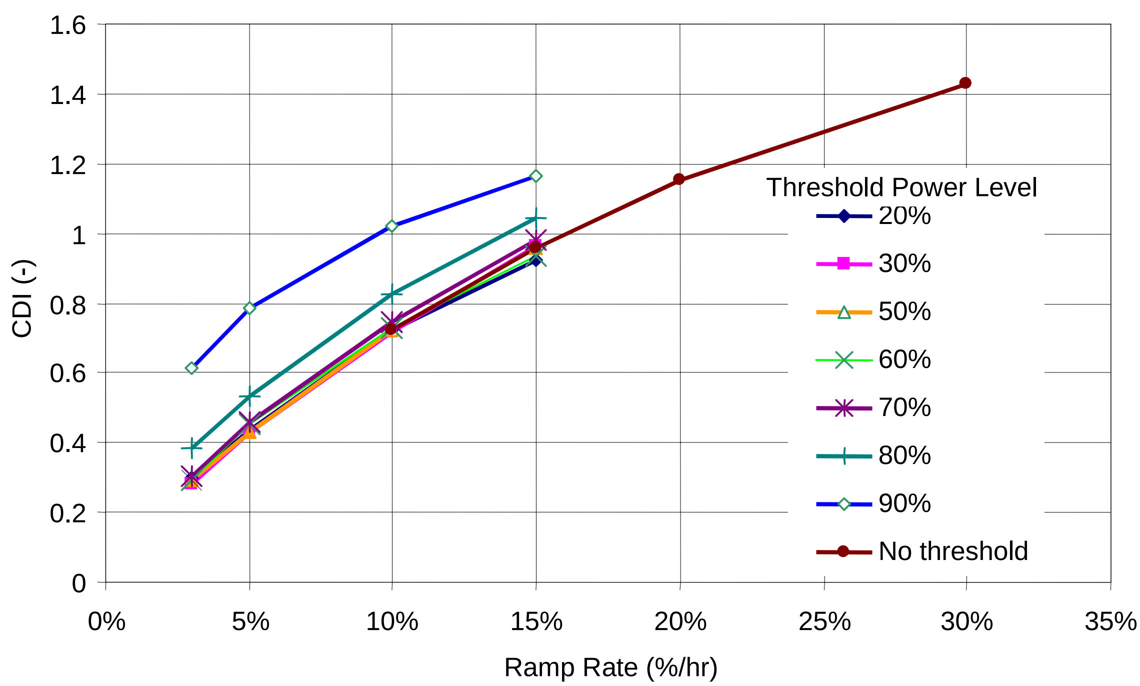

Figure 3-2
Cumulative Damage Index as a Function of Post-Threshold Ramp Rate for Zr-4 Cladding (Pre-threshold Ramp Rate = 30%/hr)

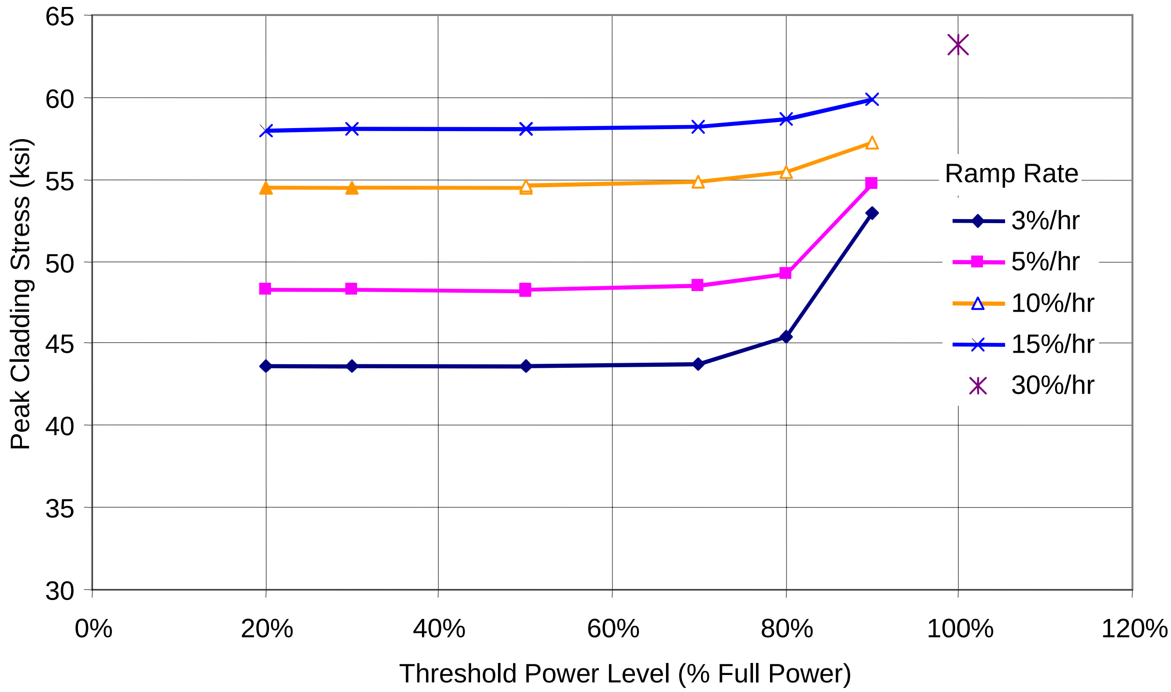

Figure 3-3
Peak Hoop Stress as a Function of Threshold Power Level for Zr-4 Cladding (Pre-threshold Ramp Rate = 30%/hr)

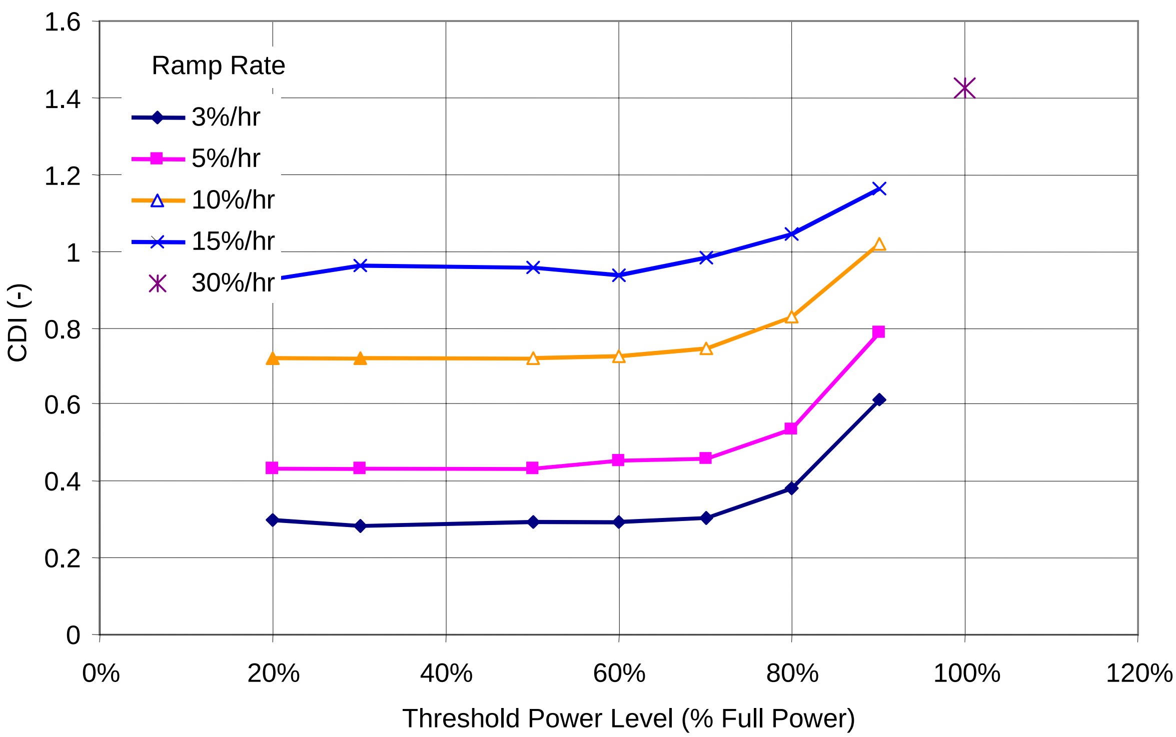

Figure 3-4
Cumulative Damage Index as a Function of Threshold Power Level for Zr-4 Cladding (Pre-threshold Ramp Rate = 30%/hr)

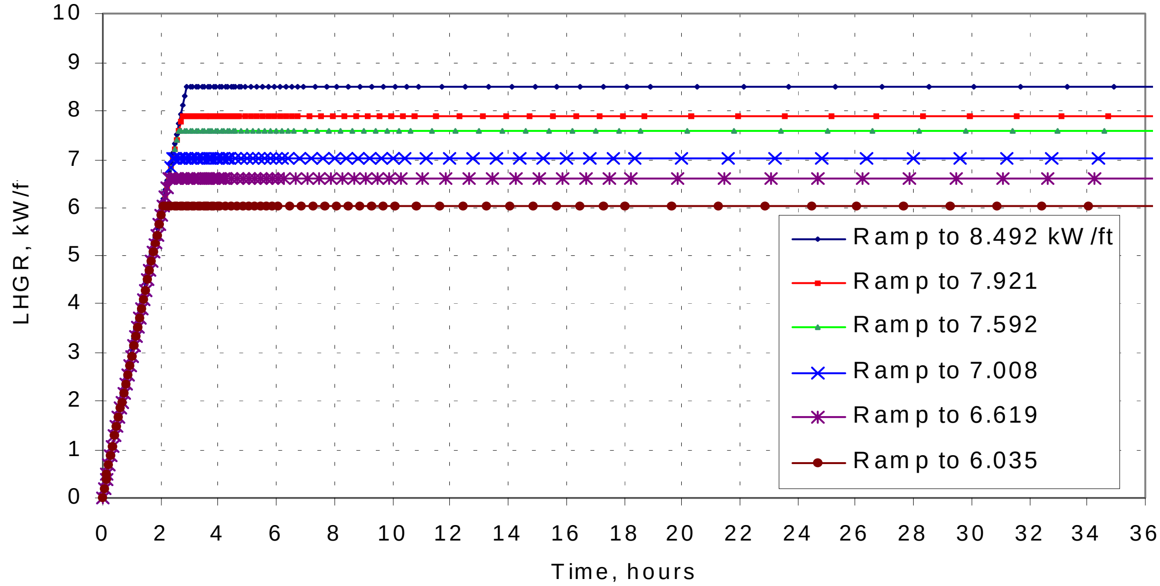

Figure 3-5
Linear Power as a Function of Time for Power Ramps to Various Terminal Power Levels for Rod E4 with Zircaloy 4 Cladding (Ramp Rate = 30%/hr, or 2.92 kW/ft/hr)

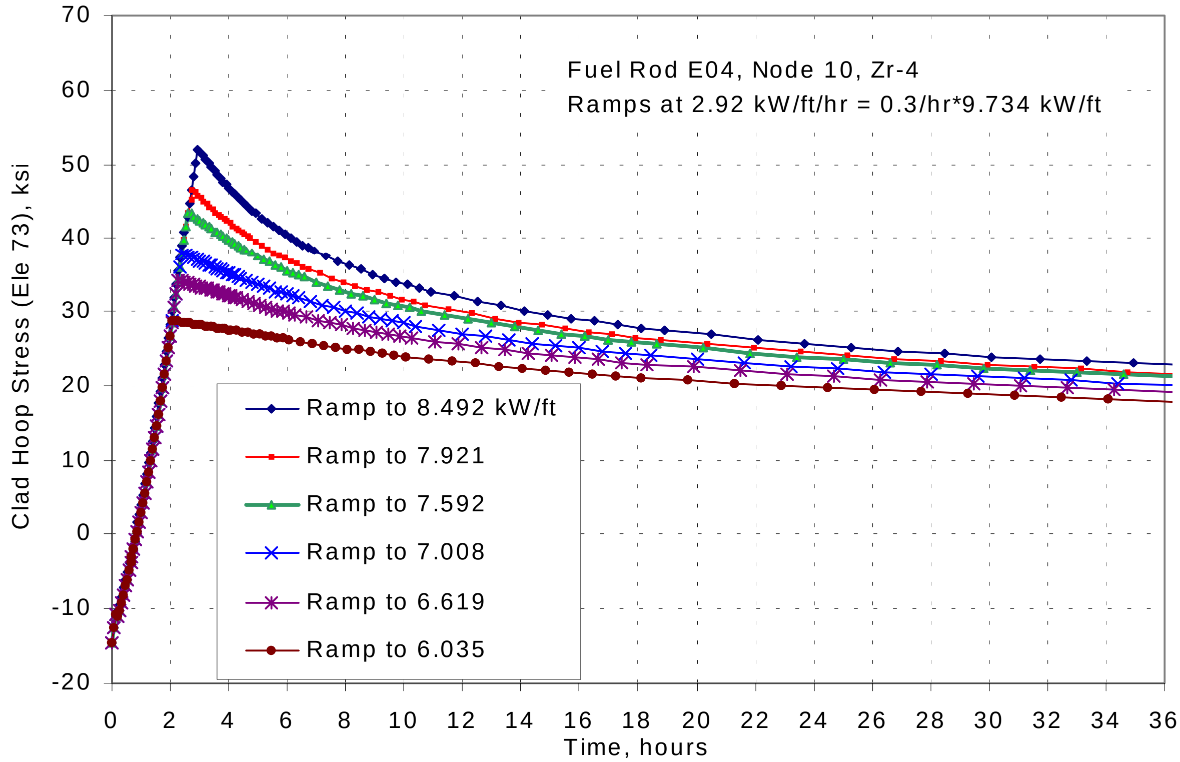

Figure 3-6
Cladding Hoop Stress as a Function of Time for Power Ramps to Various Terminal Power Levels for Rod E4 with Zircaloy 4 Cladding (Ramp Rate = 30%/hr, or 2.92 kW/ft/hr)

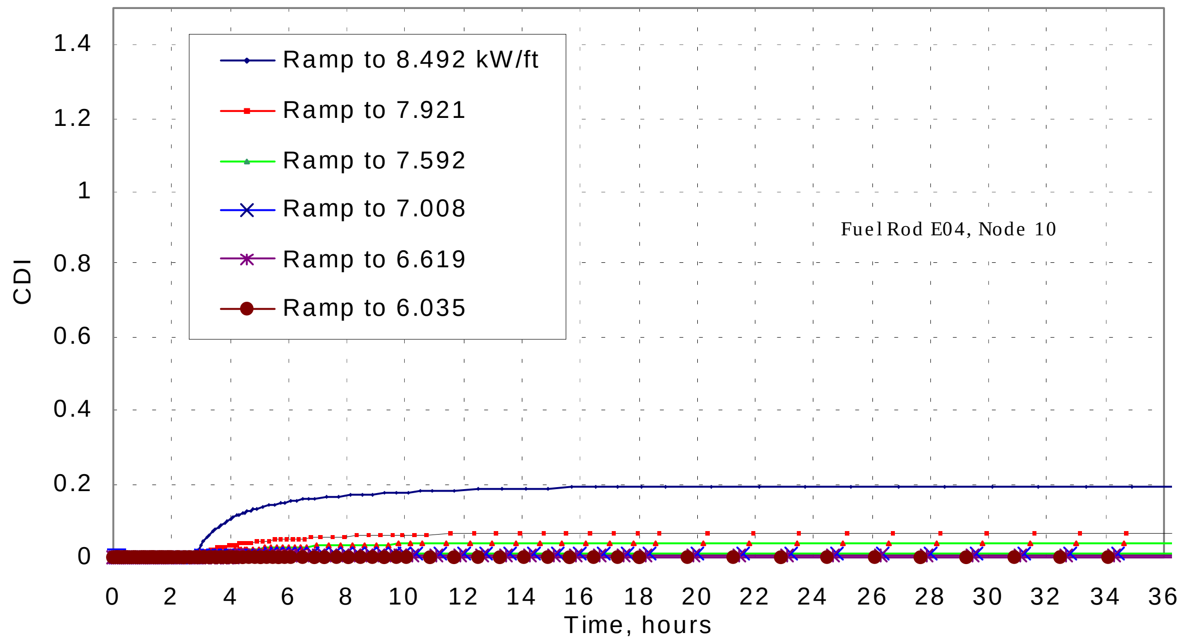

Figure 3-7
CDI as a Function of Time for Power Ramps to Various Terminal Power Levels for Rod E4 with Zircaloy 4 Cladding (Ramp Rate = 30%/hr, or 2.92 kW/ft/hr)

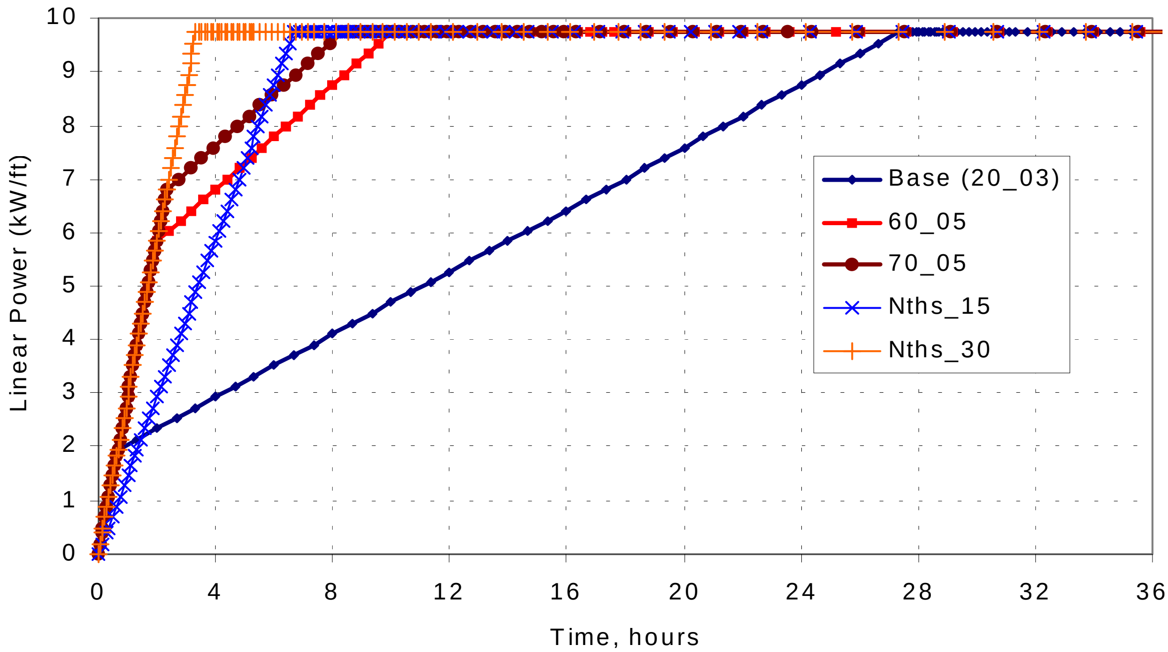

Figure 3-8
Linear Power as a Function of Time for Various Start-Up Power Ascension Regimes for Rod E4 with Zircaloy-4 Cladding

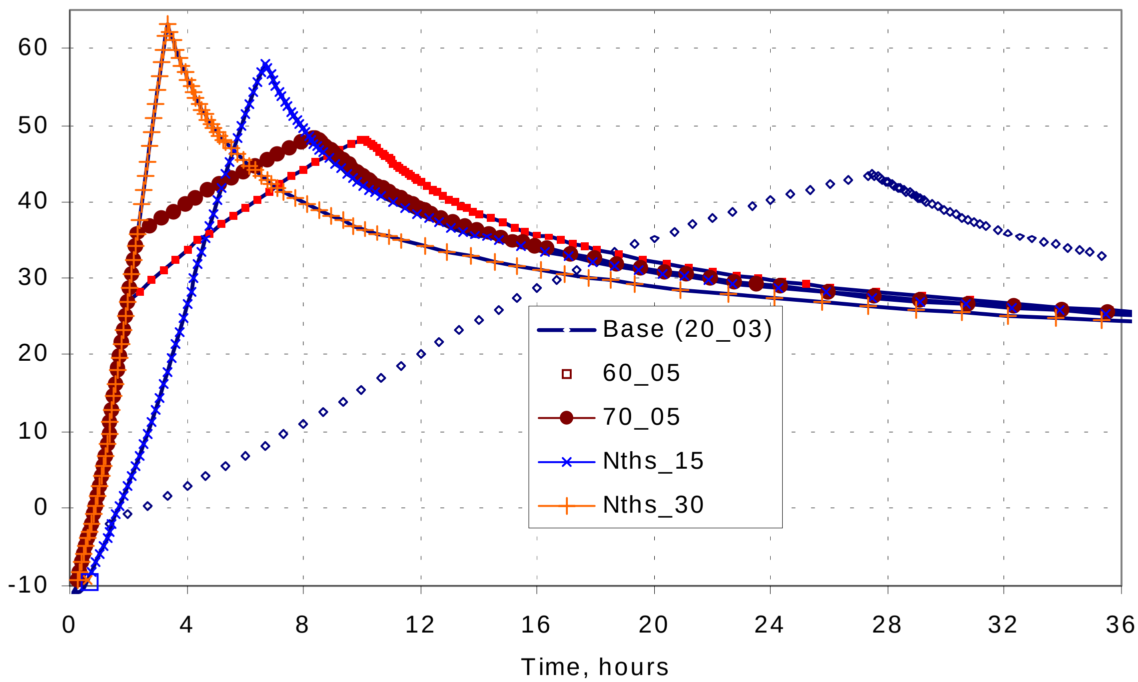

Figure 3-9
Cladding Hoop Stress as a Function of Time for Various Start-Up Power Ascension Regimes to a Local Full Power (9.734 kW/ft) for Rod E4 with Zircaloy-4 Cladding

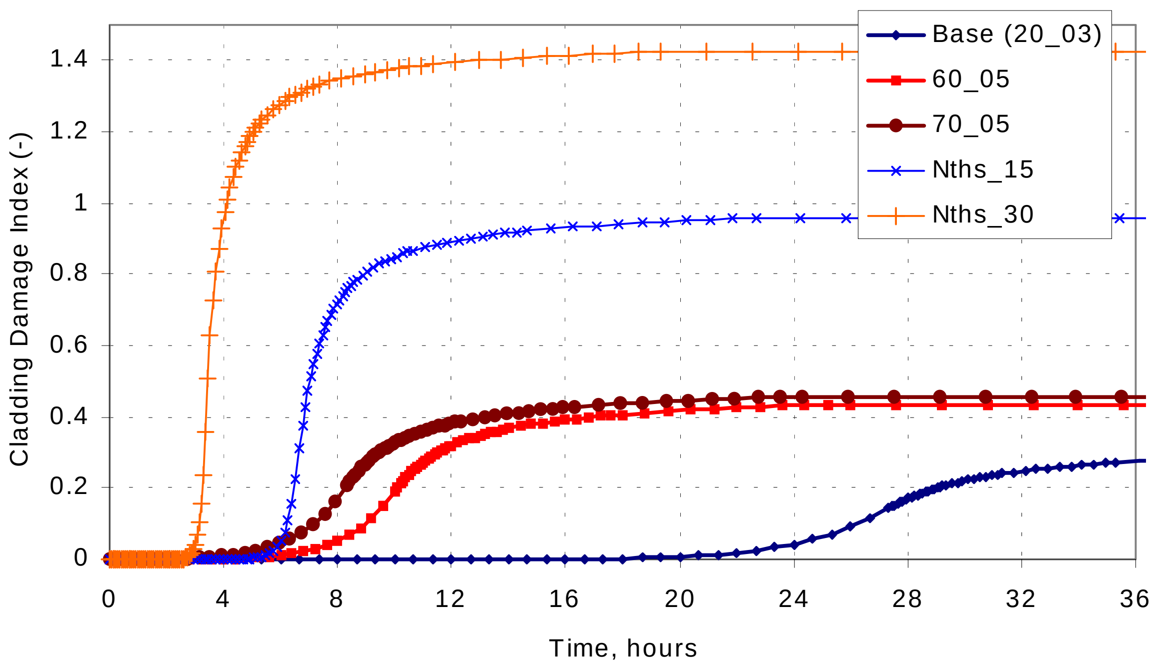

Figure 3-10
CDI as a Function of Time for Various Start-Up Power Ascension Regimes to a Local Full Power (9.734 kW/ft) for Rod E4 with Zircaloy-4 Cladding

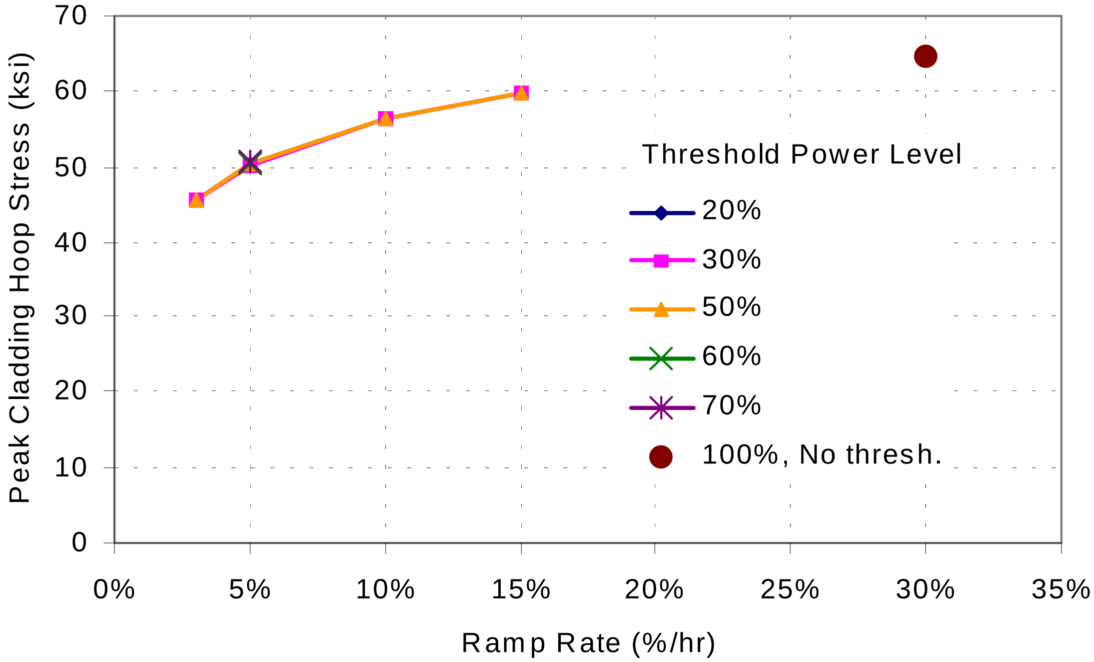

Figure 3-11
Peak Cladding Hoop Stress as a Function of Post-Threshold Ramp Rate of ZIRLO Cladding (Pre-threshold Ramp Rate = 30%/hr)

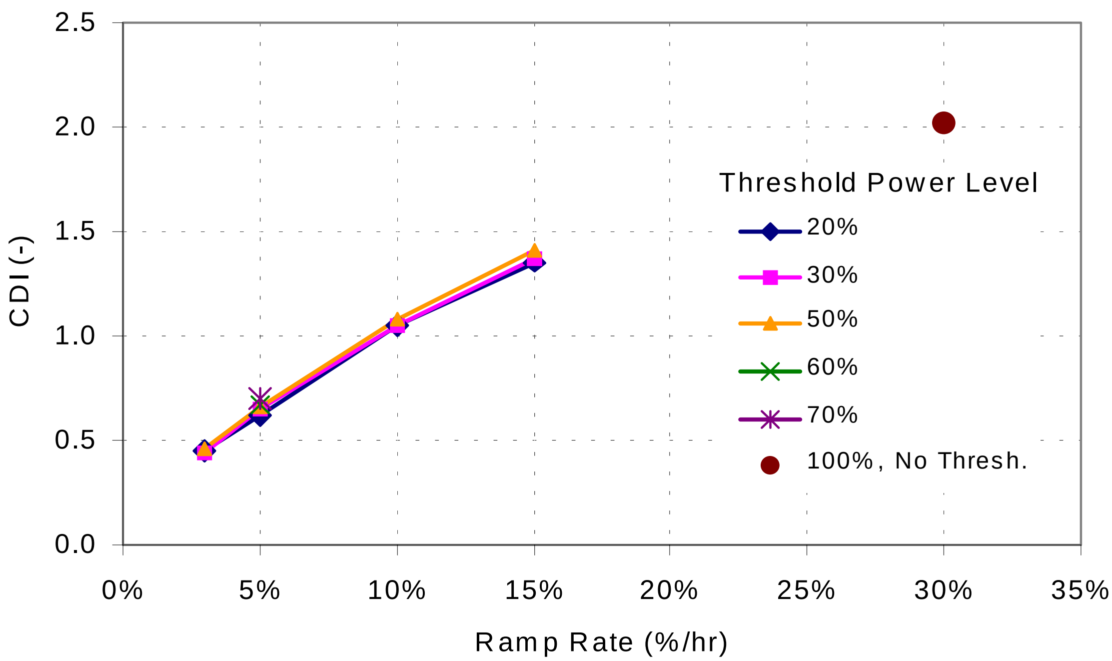

Figure 3-12
Cumulative Damage Index as a Function of Post-Threshold Ramp Rate for ZIRLO Cladding (Pre-threshold Ramp Rate = 30%/hr)

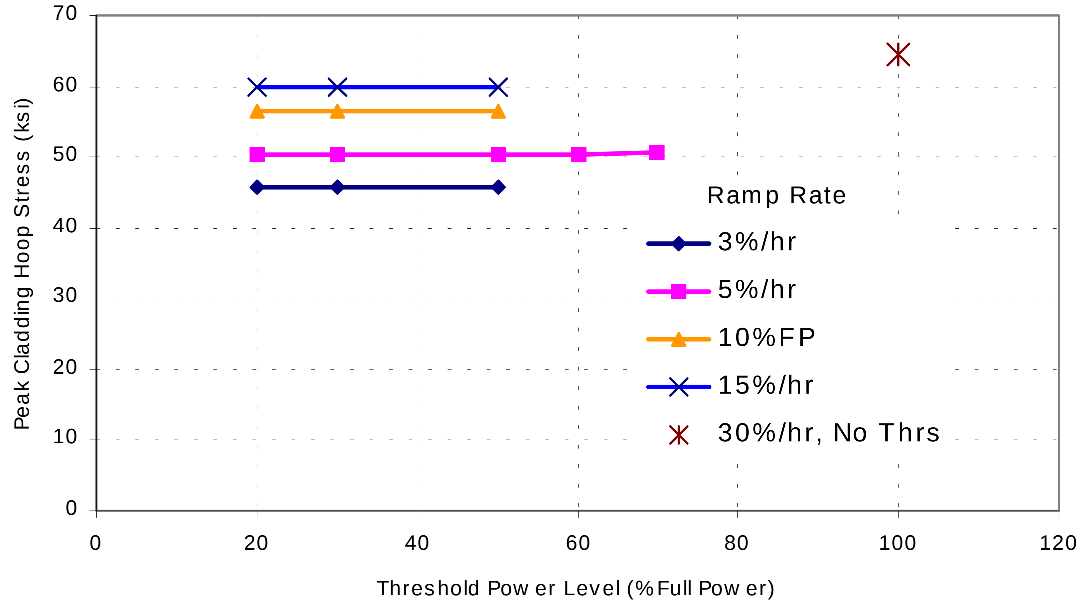

Figure 3-13
Peak Hoop Stress as a Function of Threshold Power Level for ZIRLO Cladding (Pre-threshold Ramp Rate = 30%/hr)

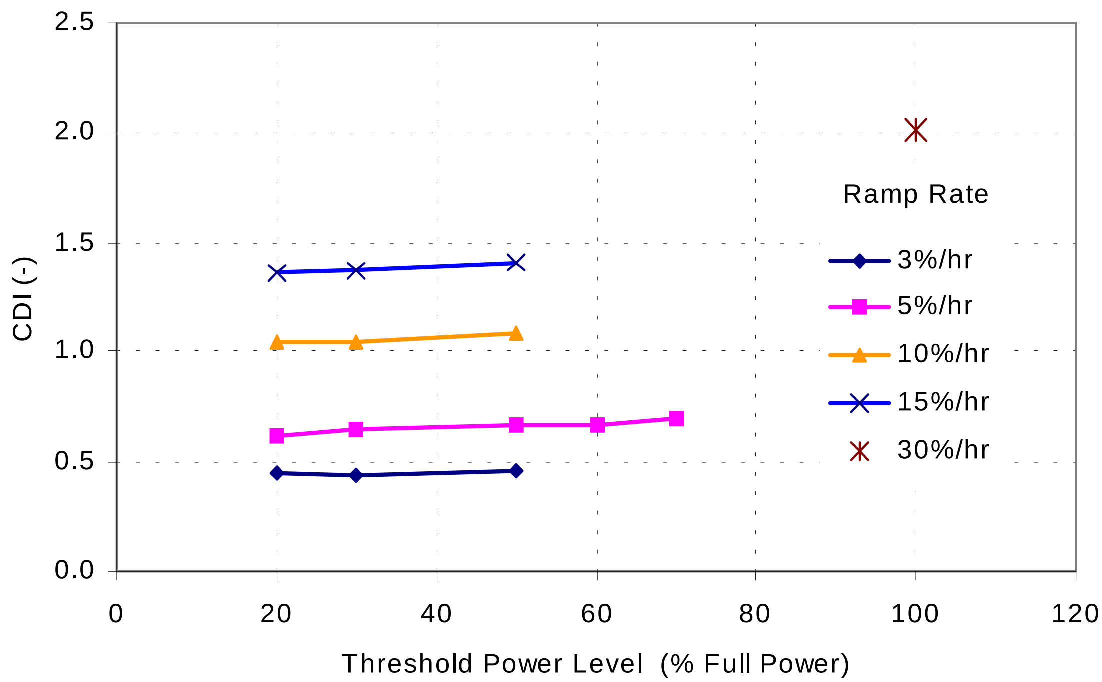

Figure 3-14
Cumulative Damage Index as a Function of Post-Threshold Ramp Rate for ZIRLO Cladding (Pre-threshold Ramp Rate = 30%/hr)

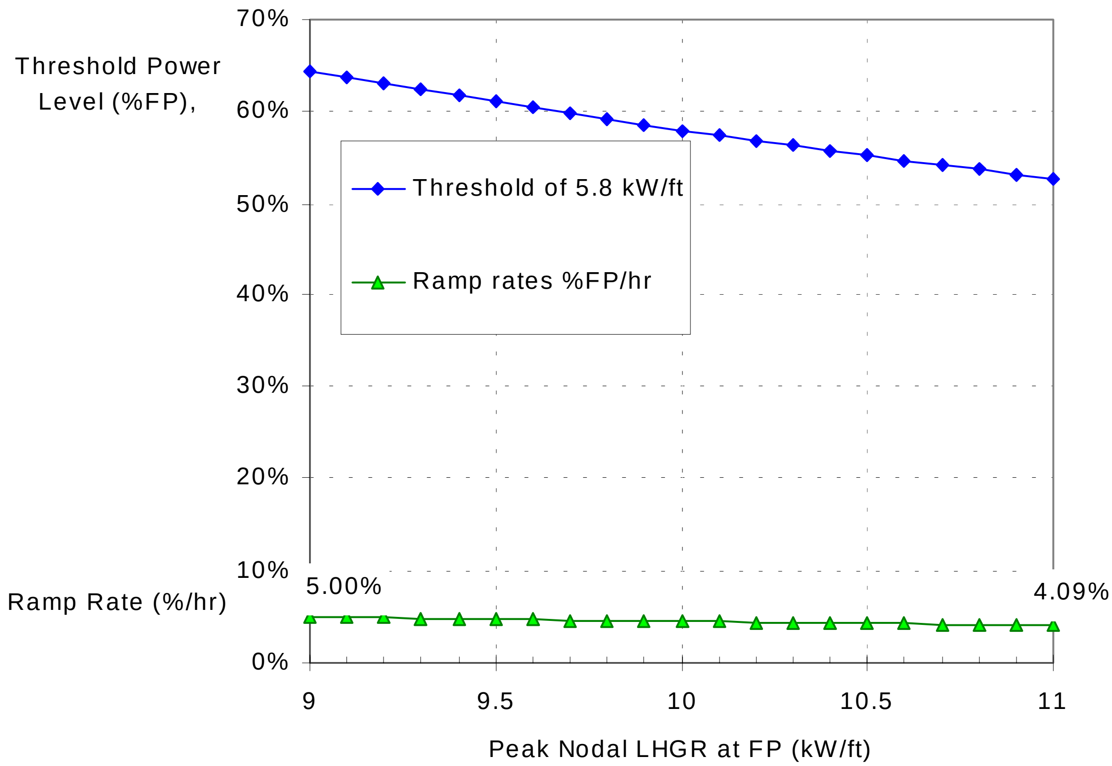

Figure 3-15
Startup Threshold and Ramp Rate as a Function of Peak Nodal Power for Once-Burned Fuel in 17x17 Fuel, with Zircaloy-4 or ZIRLO Cladding, in Catawba and McGuire Units

4
CONCLUSIONS AND RECOMMENDATIONS

The PCI response of the Westinghouse 17x17-RFA fuel rod design during PWR startup power ramps was analyzed using the FALCON fuel performance code. Analyses were conducted for both once-burned and twice-burned fuel rods under a variety of power conditions. The results of this evaluation are consistent with those of previous work [Ref. 2], particularly those involving a similar 17x17 fuel design in Yonggwang 2. The current work extends the PCI analyses to include ZIRLO cladding in addition to Zircaloy-4 and expands the evaluation to a wider spectrum of power thresholds and ramp rates.

The results demonstrate that the common practice of using a threshold of 20% FP with a post-threshold power ramp rate of 3%/hr is conservative with substantial margin to PCI failure. The analyses show that an increase in peak cladding stresses occur above a threshold of approximately 70% FP at the same post-threshold ramp rate of 3%/hr. Similarly, the cladding stresses only increase slightly when the ramp rate is increased to approximately 5%/hr for threshold values below 70% FP.

Base irradiation conditions of once-burned and twice-burned fuel rods were established through modeling the performance of full-length fuel rods under steady-state (normal base load) operation with ESCORE. These base irradiation conditions were used to initialize the PCI analyses performed with FALCON. Several coastdowns, with power reductions to 89%, 80%, 75% and 60% of full core power, were applied at the end of the first cycle in order to determine the effect of the power reduction during coastdown on the fuel-cladding gap and cladding dimensions. Of the several coastdowns evaluated for the steady-state cases, the coastdown to 60% FP produces the greatest cladding stress and CDI under subsequent startup conditions according to the PCI analyses.

Based on a relative comparison of the peak cladding stress and the cumulative damage index (CDI), a threshold of 60% FP is acceptable with a post-threshold (or restricted) ramp rate that is limited to 5%/hr for Zircaloy-4 cladding. This threshold corresponds to a local linear power of 5.8 kW/ft on the basis of a peak nodal linear power of 9.734 kW/ft and the ramp rate of 5%/hr is equivalent to a linear power rate increase of 0.487 kW/ft/hr. If the nodal linear power is greater at full power conditions, then the threshold or ramp rate may have to be reduced. Certainly, for both Zircaloy-4 and ZIRLO cladding, the results of the study support a threshold power level of 40 to 50% of full power with a ramp rate limited to 5%/hr.

The threshold in terms of %FP and ramp rate in terms of %FP/hr is actually a function of the peak nodal power at full power. These relationship are illustrated in Figure 3-15 which provides the threshold and ramp rate as functions of local (nodal) linear power at the full power condition.

These could be translated to assembly radial power if the appropriate bounding peaking factors are known.

The PCI analyses were based on the condition of the fuel and cladding following a coastdown to 60%FP over a period of 60 days (at a power descension rate of 1%FP/1.5 calendar day). A limited sensitivity calculation showed that the lower the power level at the end of coastdown, the higher the stresses in the cladding during a subsequent startup. Extended coastdowns beyond those addressed in this study may require a lower threshold. Additional analyses are to establish the optimum startup power threshold and ramp rate restrictions.

5
REFERENCES

1. J. Trotter, D. Sunderland, W. Lyon and R. Montgomery, "PWR Restart Ramp Rate Restrictions," EPRI TR-112140-V1, April 1999.

2. Y. B. Kim, R. O. Montgomery and W. F. Lyon, "Effect of Startup Ramp Rate on Pellet-Cladding Interaction of PWR Fuel Rods," EPRI TR-112140-V2, January 1998.

3. R. B. Fancher, et al, "ESCORE: The EPRI Steady-State Core Reload Evaluator Code, Volume 1: Theory Manual," EPRI Report NP-4492-CCMP, Volume 1, August 1986.

4. M. A. Krammen, et al, "ESCORE: The EPRI Steady-State Core Reload Evaluator Code, Volume 2: User's Manual," EPRI Report NP-4492-CCMP, Volume 2, August 1986.

5. Y. R. Rashid, et al, "Modelling of PCI Under Steady State and Transient Operating Conditions," Water Reactor Fuel Element Computer Modelling in Steady State, Transient and Accident Conditions, IAEA Report IWGFPT/32, Proceedings of a Technical Committee Meeting, Preston, UK, Sep 1988.

6. J. T. A. Roberts, et al, "A Stress Corrosion Cracking Model for Pellet-Cladding Interaction Failures in Light Water Reactor Fuel Pellets," Proceedings of the 4th International Conference on Zirconium in the Nuclear Industry, ASTM STP 681, June, 1978.

7. Y. R. Rashid, et al, "FREY-01: Fuel Rod Evaluation System, Vol. 1: Theory Manual," EPRI Report NP-3277, Vol. 1, August 1994.

8. Y. R. Rashid, et al, "FREY-01: Fuel Rod Evaluation System, Vol. 2: User's Manual," EPRI Report NP-3277, Vol. 2, August 1994.

9. George P. Sabol, et al, ASTM-1245, "In-Reactor Corrosion Performance of ZIRLO and Zircaloy-4", Zirconium in the Nuclear Industry: 10th International Symposium, ASTM STP 1245, pp 724-744, 1994.

10. D. G. Franklin, "Zircaloy-4 Cladding Deformation During Power Reactor Irradiation," Zirconium in the Nuclear Industry: Fifth Conference, ASTM STP 754, D. G. Franklin, Ed., American Society for Testing and Materials, pp. 235-267, 1982.

11. Communication from T. Saville (Duke) to D. Sunderland (ANATECH), Document CNC-1553.05-00-0327, Rev 2, Corr 2 in CNEI-0400-29, Rev. 11

A
APPENDIX A

Table A-1
Normalized Axial Power Shapes for Rod E04

	Tube Sheet, EFPD															
Node	1, 4	2, 12	3, 25	4, 50	5, 100	6, 150	7, 200	8, 250	9, 300	10, 350	11, 400	12, 450	13, 470	14, 480	15, 490	16, 494
24	0.200	0.207	0.212	0.221	0.246	0.271	0.294	0.317	0.341	0.367	0.398	0.428	0.443	0.462	0.492	0.291
23	0.524	0.539	0.546	0.564	0.610	0.650	0.684	0.717	0.750	0.786	0.826	0.858	0.875	0.910	0.970	0.628
22	0.693	0.708	0.716	0.735	0.783	0.820	0.851	0.880	0.907	0.936	0.969	0.990	1.004	1.040	1.106	0.779
21	0.843	0.858	0.866	0.885	0.928	0.960	0.984	1.005	1.025	1.046	1.069	1.079	1.088	1.124	1.190	0.898
20	0.938	0.951	0.957	0.974	1.009	1.032	1.047	1.061	1.072	1.085	1.098	1.099	1.104	1.136	1.197	0.966
19	0.996	1.007	1.011	1.025	1.050	1.064	1.072	1.078	1.083	1.088	1.094	1.088	1.090	1.118	1.172	1.013
18	1.038	1.046	1.049	1.058	1.074	1.080	1.082	1.082	1.081	1.081	1.080	1.070	1.070	1.094	1.139	1.062
17	1.098	1.103	1.104	1.111	1.118	1.116	1.113	1.108	1.103	1.098	1.092	1.079	1.077	1.097	1.134	1.093
16	1.132	1.134	1.133	1.137	1.135	1.128	1.120	1.113	1.104	1.095	1.085	1.071	1.068	1.083	1.111	1.127
15	1.130	1.130	1.128	1.128	1.120	1.109	1.098	1.089	1.078	1.067	1.054	1.041	1.036	1.047	1.066	1.139
14	1.185	1.182	1.179	1.176	1.161	1.146	1.132	1.120	1.106	1.093	1.077	1.063	1.057	1.063	1.073	1.171
13	1.206	1.201	1.197	1.192	1.172	1.153	1.138	1.124	1.109	1.094	1.076	1.062	1.055	1.056	1.058	1.189
12	1.202	1.194	1.190	1.183	1.159	1.139	1.123	1.109	1.094	1.078	1.059	1.046	1.038	1.035	1.029	1.193
11	1.223	1.214	1.209	1.200	1.173	1.152	1.136	1.121	1.105	1.089	1.069	1.056	1.047	1.039	1.025	1.219
10	1.243	1.233	1.228	1.218	1.189	1.167	1.150	1.135	1.120	1.103	1.082	1.069	1.060	1.047	1.025	1.225
9	1.245	1.234	1.230	1.218	1.189	1.168	1.152	1.138	1.123	1.106	1.086	1.074	1.065	1.047	1.016	1.222
8	1.215	1.205	1.200	1.188	1.161	1.142	1.128	1.115	1.102	1.087	1.070	1.060	1.051	1.029	0.992	1.206
7	1.240	1.231	1.227	1.214	1.188	1.171	1.158	1.146	1.134	1.120	1.104	1.095	1.087	1.060	1.014	1.203
6	1.225	1.216	1.213	1.201	1.178	1.164	1.154	1.144	1.135	1.124	1.112	1.106	1.100	1.069	1.016	1.176
5	1.165	1.158	1.155	1.144	1.127	1.118	1.112	1.106	1.102	1.096	1.090	1.089	1.086	1.053	0.995	1.117
4	1.128	1.123	1.121	1.111	1.101	1.097	1.095	1.094	1.094	1.094	1.095	1.100	1.100	1.065	1.002	1.060
3	1.021	1.018	1.016	1.009	1.005	1.008	1.011	1.015	1.021	1.028	1.038	1.052	1.057	1.022	0.959	0.947
2	0.824	0.823	0.822	0.817	0.820	0.828	0.836	0.845	0.856	0.869	0.888	0.911	0.921	0.891	0.834	0.756
1	0.286	0.288	0.290	0.292	0.303	0.316	0.328	0.341	0.355	0.371	0.391	0.414	0.424	0.411	0.384	0.320

Table A-2
Normalized Axial Power Shapes for Rod Q17

	Tube Sheet, EFPD															
Node	1, 4	2, 12	3, 25	4, 50	5, 100	6, 150	7, 200	8, 250	9, 300	10, 350	11, 400	12, 450	13, 470	14, 480	15, 490	16, 494
24	0.200	0.207	0.212	0.221	0.246	0.271	0.294	0.317	0.341	0.367	0.398	0.428	0.443	0.462	0.492	0.291
23	0.524	0.539	0.546	0.564	0.610	0.650	0.684	0.717	0.750	0.786	0.826	0.858	0.875	0.910	0.970	0.628
22	0.693	0.708	0.716	0.735	0.783	0.820	0.851	0.880	0.907	0.936	0.969	0.990	1.004	1.040	1.106	0.779
21	0.843	0.858	0.866	0.885	0.928	0.960	0.984	1.005	1.025	1.046	1.069	1.079	1.088	1.124	1.190	0.898
20	0.938	0.951	0.957	0.974	1.009	1.032	1.047	1.061	1.072	1.085	1.098	1.099	1.104	1.136	1.197	0.966
19	0.996	1.007	1.011	1.025	1.050	1.064	1.072	1.078	1.083	1.088	1.094	1.088	1.090	1.118	1.172	1.013
18	1.038	1.046	1.049	1.058	1.074	1.080	1.082	1.082	1.081	1.081	1.080	1.070	1.070	1.094	1.139	1.062
17	1.098	1.103	1.104	1.111	1.118	1.116	1.113	1.108	1.103	1.098	1.092	1.079	1.077	1.097	1.134	1.093
16	1.132	1.134	1.133	1.137	1.135	1.128	1.120	1.113	1.104	1.095	1.085	1.071	1.068	1.083	1.111	1.127
15	1.130	1.130	1.128	1.128	1.120	1.109	1.098	1.089	1.078	1.067	1.054	1.041	1.036	1.047	1.066	1.139
14	1.185	1.182	1.179	1.176	1.161	1.146	1.132	1.120	1.106	1.093	1.077	1.063	1.057	1.063	1.073	1.171
13	1.206	1.201	1.197	1.192	1.172	1.153	1.138	1.124	1.109	1.094	1.076	1.062	1.055	1.056	1.058	1.189
12	1.202	1.194	1.190	1.183	1.159	1.139	1.123	1.109	1.094	1.078	1.059	1.046	1.038	1.035	1.029	1.193
11	1.223	1.214	1.209	1.200	1.173	1.152	1.136	1.121	1.105	1.089	1.069	1.056	1.047	1.039	1.025	1.219
10	1.243	1.233	1.228	1.218	1.189	1.167	1.150	1.135	1.120	1.103	1.082	1.069	1.060	1.047	1.025	1.225
9	1.245	1.234	1.230	1.218	1.189	1.168	1.152	1.138	1.123	1.106	1.086	1.074	1.065	1.047	1.016	1.222
8	1.215	1.205	1.200	1.188	1.161	1.142	1.128	1.115	1.102	1.087	1.070	1.060	1.051	1.029	0.992	1.206
7	1.240	1.231	1.227	1.214	1.188	1.171	1.158	1.146	1.134	1.120	1.104	1.095	1.087	1.060	1.014	1.203
6	1.225	1.216	1.213	1.201	1.178	1.164	1.154	1.144	1.135	1.124	1.112	1.106	1.100	1.069	1.016	1.176
5	1.165	1.158	1.155	1.144	1.127	1.118	1.112	1.106	1.102	1.096	1.090	1.089	1.086	1.053	0.995	1.117
4	1.128	1.123	1.121	1.111	1.101	1.097	1.095	1.094	1.094	1.094	1.095	1.100	1.100	1.065	1.002	1.060
3	1.021	1.018	1.016	1.009	1.005	1.008	1.011	1.015	1.021	1.028	1.038	1.052	1.057	1.022	0.959	0.947
2	0.824	0.823	0.822	0.817	0.820	0.828	0.836	0.845	0.856	0.869	0.888	0.911	0.921	0.891	0.834	0.756
1	0.286	0.288	0.290	0.292	0.303	0.316	0.328	0.341	0.355	0.371	0.391	0.414	0.424	0.411	0.384	0.320

About EPRI

EPRI creates science and technology solutions for the global energy and energy services industry. U.S. electric utilities established the Electric Power Research Institute in 1973 as a nonprofit research consortium for the benefit of utility members, their customers, and society. Now known simply as EPRI, the company provides a wide range of innovative products and services to more than 1000 energy-related organizations in 40 countries. EPRI's multidisciplinary team of scientists and engineers draws on a worldwide network of technical and business expertise to help solve today's toughest energy and environmental problems.

EPRI. Electrify the World

Program: 1000847

Nuclear Power

Printed on recycled paper in the United States of America

EPRI • 3412 Hillview Avenue, Palo Alto, California 94304 • PO Box 10412, Palo Alto, California 94303 • USA
800.313.3774 • 650.855.2121 • askepri@epri.com • www.epri.com